Geochemistry Geophysics Geosystems G3
AN ELECTRONIC JOURNAL OF THE EARTH SCIENCES
Published by AGU and the Geochemical Society

Article
Volume 7, Number 6
21 June 2006
Q06016, doi:10.1029/2005GC001109
ISSN: 1525-2027

Detachment shear zone of the Atlantis Massif core complex, Mid-Atlantic Ridge, 30°N

J. A. Karson
Division of Earth and Ocean Sciences, Duke University, Durham, North Carolina 27708, USA

Now at Department of Earth Sciences, 204 Heroy Geology Laboratory, Syracuse University, Syracuse, New York 13244-1070, USA (jakarson@syr.edu)

G. L. Früh-Green
Department of Earth Sciences, ETH-Zurich, CH-8092, Zürich, Switzerland

D. S. Kelley
School of Oceanography, University of Washington, Seattle, Washington 98195, USA

E. A. Williams
Division of Earth and Ocean Sciences, Duke University, Durham, North Carolina 27708, USA

D. R. Yoerger and M. Jakuba
Woods Hole Oceanographic Institution, Woods Hole, Massachusetts 02543, USA

[1] Near-bottom investigations of the cross section of the Atlantis Massif exposed in a major tectonic escarpment provide an unprecedented view of the internal structure of the footwall domain of this oceanic core complex. Integrated direct observations, sampling, photogeology, and imaging define a mylonitic, low-angle detachment shear zone (DSZ) along the crest of the massif. The shear zone may project beneath the nearby, corrugated upper surface of the massif. The DSZ and related structures are inferred to be responsible for the unroofing of upper mantle peridotites and lower crustal gabbroic rocks by extreme, localized tectonic extension during seafloor spreading over the past 2 m.y. The DSZ is characterized by strongly foliated to mylonitic serpentinites and talc-amphibole schists. It is about 100 m thick and can be traced continuously for at least 3 km in the tectonic transport direction. The DSZ foliation arches over the top of the massif in a convex-upward trajectory mimicking the morphology of the top of the massif. Kinematic indicators show consistent top-to-east (toward the MAR axis) tectonic transport directions. Foliated DSZ rocks grade structurally downward into more massive basement rocks that lack a pervasive outcrop-scale foliation. The DSZ and underlying basement rocks are cut by discrete, anastomosing, normal-slip, shear zones. Widely spaced, steeply dipping, normal faults cut all the older structures and localize serpentinization-driven hydrothermal outflow at the Lost City Hydrothermal Field. A thin (few meters) sequence of sedimentary breccias grading upward into pelagic limestones directly overlies the DSZ and may record a history of progressive rotation of the shear zone from a moderately dipping attitude into its present, gently dipping orientation during lateral spreading and uplift.

Components: 15,217 words, 19 figures, 2 tables.

Keywords: detachment faults; faults; oceanic core complex; seafloor spreading; serpentinite; shear zones.

Index Terms: 3035 Marine Geology and Geophysics: Midocean ridge processes; 8010 Structural Geology: Fractures and faults; 8012 Structural Geology: High strain deformation zones.

Received 7 August 2005; **Revised** 10 March 2006; **Accepted** 31 March 2006; **Published** 21 June 2006.

Karson, J. A., G. L. Früh-Green, D. S. Kelley, E. A. Williams, D. R. Yoerger, and M. Jakuba (2006), Detachment shear zone of the Atlantis Massif core complex, Mid-Atlantic Ridge, 30°N, *Geochem. Geophys. Geosyst.*, *7*, Q06016, doi:10.1029/2005GC001109.

1. Introduction

[2] Extreme extension of oceanic lithosphere during seafloor spreading creates oceanic core complexes (OCCs) defined by broad, elevated massifs (few tens of kilometers across) where deep crustal and in some cases upper mantle rocks have been unroofed and uplifted [*Karson*, 1990; *Mutter and Karson*, 1992; *Tucholke et al.*, 1998; *Blackman et al.*, 2002; *Reston et al.*, 2002]. The upper surfaces of these massifs are commonly characterized by gently sloping, broadly arched surfaces marked by spreading-parallel corrugations and finer scale striations interpreted as major, low-angle detachment shear zones [*Cann et al.*, 1997; *Tucholke et al.*, 1998; *Escartín and Cannat*, 1999; *Reston et al.*, 2002; *Searle et al.*, 2003; *Okino et al.*, 2004]. The dimensions of these surfaces in the spreading direction suggest that these shear zones accommodate as much as a few tens of kilometers of displacement over 1–2 m.y. Such long-lived structures have been referred to as "megamullions" to differentiate them from other OCCs [*Tucholke et al.*, 1998]. In the absence of significant magmatic construction, major detachment shear zones may essentially define the divergent plate boundary for as much as 2 m.y. Major corrugated surfaces appear to dip beneath faulted upper crustal units [e.g., *Blackman et al.*, 2002] and locally may define the walls of the median valley of spreading centers [*Karson and Dick*, 1983; *Karson et al.*, 1987; *Mutter and Karson*, 1992]. These major surfaces are truncated by spreading-center-parallel lineaments ("terminations") created by faulting, magmatic construction or a combination of these processes [*Karson*, 1990; *Tucholke et al.*, 1998; *Searle et al.*, 2003; *Okino et al.*, 2004].

[3] Fault rocks are commonly recovered from the corrugated tops of OCCs, but this in itself does not require detachment faulting. Mafic to ultramafic plutonic rocks that make up these massifs initially formed at some depth in the crust or mantle and must have been exhumed from beneath a substantial thickness of upper crustal material by faulting. High-angle faults in thin magmatic crust [*Cannat*, 1993] or conjugate faulting [*White and Stroup*, 1979] could also potentially expose deep-level rocks. To date, the specifics of the geometry and kinematics of major detachment faults in oceanic core complexes have remained elusive issues.

[4] Perhaps the most compelling case for a major low-angle detachment fault comes from sampling with a rock drill across the top of a corrugated surface of an OCC near 15°45′N on the Mid-Atlantic Ridge (MAR) [*MacLeod et al.*, 2002; *Escartín et al.*, 2003]. This study recovered distinctive serpentinite and talc-rich fault rocks cropping out systematically in relatively shallow exposures and less faulted rocks in deeper exposures, suggesting that the fault rocks belong to a subhorizontal shear zone about 100 m thick. Elsewhere, submersible dives on the edge of an OCC defining the median valley wall of the MAR near the Kane Transform Fault (MARK area) have mapped an extensive, low-angle shear zone essentially defining the wall of the median valley of the MAR and interpreted as a youthful detachment fault that has yet to be rotated into a subhorizontal orientation [*Karson and Dick*, 1983; *Karson*, 1990; *Mével et al.*, 1991; *Karson and Lawrence*, 1997b]. Deep crustal drilling into a gabbroic OCC on the Southwest Indian Ridge has also penetrated a major shear zone related to detachment faulting [*Dick et al.*, 1991, 2000]. Other efforts to investigate detachment faults on corrugated surfaces of OCCs have been hampered by the extensive sediment cover over the basement [*Tucholke et al.*, 2001; *Blackman et al.*, 2002; *Searle et al.*, 2003].

[5] In this study, we use the integrated results of direct observations and sampling from the submersible *Alvin*, photogeology from near-bottom digital images from the Remotely Operated Vehicle (ROV) *Argo II*, and high-resolution SM2000 bathymetry collected with the Autonomous Benthic Explorer (*ABE*), to map a laterally continuous detachment shear zone (DSZ) and related structures along the top of the Atlantis Massif OCC. Our results reveal important geological features relevant to the tectonic and hydrothermal history of the Atlantis Massif that may be significant for OCCs elsewhere. Understanding the details of detachment shear zones in OCCs and their geolog-

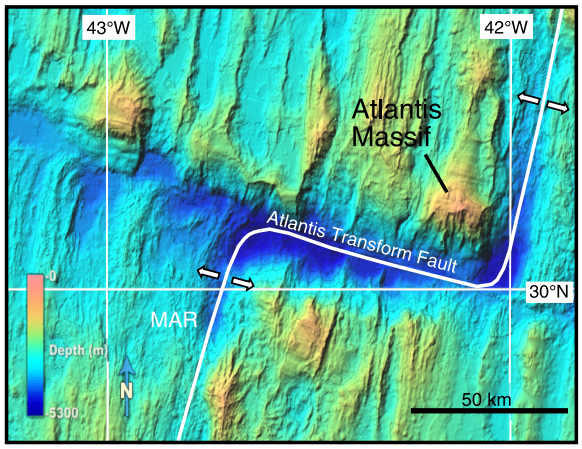

Figure 1. Plate boundary geometry and seafloor morphology near the intersection of the Mid-Atlantic Ridge (MAR) and the Atlantis Transform Fault. Broad, elevated massifs with spreading-parallel corrugations in this area are interpreted as oceanic core complexes. The Atlantis Massif is located at the inside corner of the ridge-transform intersection (from Center for Environmental Visualization, University of Washington).

ical relationships with surrounding rock units are essential for a more complete documentation of this style of seafloor spreading.

2. Atlantis Massif Oceanic Core Complex

[6] The Atlantis Massif is located at 30°N latitude, where it is bounded by the western median valley wall of the MAR (half-spreading rate is 12 mm/yr) and the Atlantis Transform Fault (Figures 1 and 2). Centered at ~20 km from the spreading axis, the massif is inferred to have formed over the past 1.5–2.0 m.y. [*Cann et al.*, 1997; *Blackman et al.*, 1998, 2002].

[7] Side-scan sonar surveys show that the upper surface of the central part of the massif has the strongly corrugated form typical of other OCCs. This surface is interpreted as an exposed detachment fault or "slip surface" [*Cann et al.*, 1997; *Blackman et al.*, 1998, 2002]. A prominent eastern ridge on the flank of the massif is a fault-bounded block of basaltic lavas interpreted as an allochthonous, hanging wall block atop the detachment fault. *Alvin* dives on the crest of the massif show that the corrugated surface is covered by pelagic ooze, rubble, and dispersed outcrops of sedimentary breccia with basalt and serpentinite clasts in a carbonate matrix [*Blackman et al.*, 2002; *Schroeder et al.*, 2002; *Früh-Green et al.*, 2003]. Some talc-rich fault rocks have been recovered from rubble in this area [*Blackman et al.*, 2002; *Schroeder and John*, 2004], but no outcrops of fault rocks have been found in this corrugated terrain.

[8] Seismic investigations show relatively high velocities (Vp > 7.6 km/sec) within <500 m of the upper surface of the massif suggesting that it is composed dominantly of high-density mafic and/or partially altered ultramafic material [*Collins et al.*, 2001]. Multichannel seismic reflection across the top of the massif shows prominent reflectors a few hundred meters beneath the surface interpreted as low-angle fault zones or alteration fronts [*Canales et al.*, 2004]. Recently, deep crustal drilling during IODP Legs 304 and 305 (Hole U1309D) penetrated the corrugated top of the massif. In this site, >1400 m of variably deformed and altered olivine-rich gabbroic rocks were recovered. Small amounts of ultramafic material were also recovered mainly near the top of this section. Although minor talc-rich rocks were found in some of the holes drilled during IODP Leg 304 [*Shipboard Scientific Party*, 2005a], a major detachment shear zone was not intersected in the core from Hole U1309D [*Shipboard Scientific Party*, 2005a, 2005b]. Thus available data from the central part of the massif suggest that it is composed of dominantly gabbroic material that has been unroofed by slip on a detachment fault marked by the corrugated surface (Figure 2b).

[9] Extensive exposures on the south wall of the massif, facing the Atlantis Transform Fault, provide a cross section of the footwall domain of this OCC (Figure 2b). This area is located about 5 km to the south of the strongly corrugated central part of the massif and the IODP drill site. Initial investigations of the south wall of the massif showed that it is dominated by massive serpentinized peridotite cut by local shear zones [*Blackman et al.*, 2002]. Interspersed masses of metagabbros record a history of high-temperature (800°C) deformation and recrystallization overprinted by greenschist facies metamorphism and deformation. In the ultramafic rocks, high-temperature deformation fabrics are overprinted by serpentinization and talc metasomatism in localized shear zones [*Früh-Green et al.*, 2001; *Schroeder and John*, 2004]. On the basis of increasing cataclastic deformation in samples collected near the top of the south wall, a low-angle detachment fault was inferred along the top of the massif [*Blackman et al.*, 2002; *Schroeder and John*, 2004; *Boschi et al.*, 2006].

[10] Building on previous studies, *Alvin* dives conducted in 2003 for the first time, provide

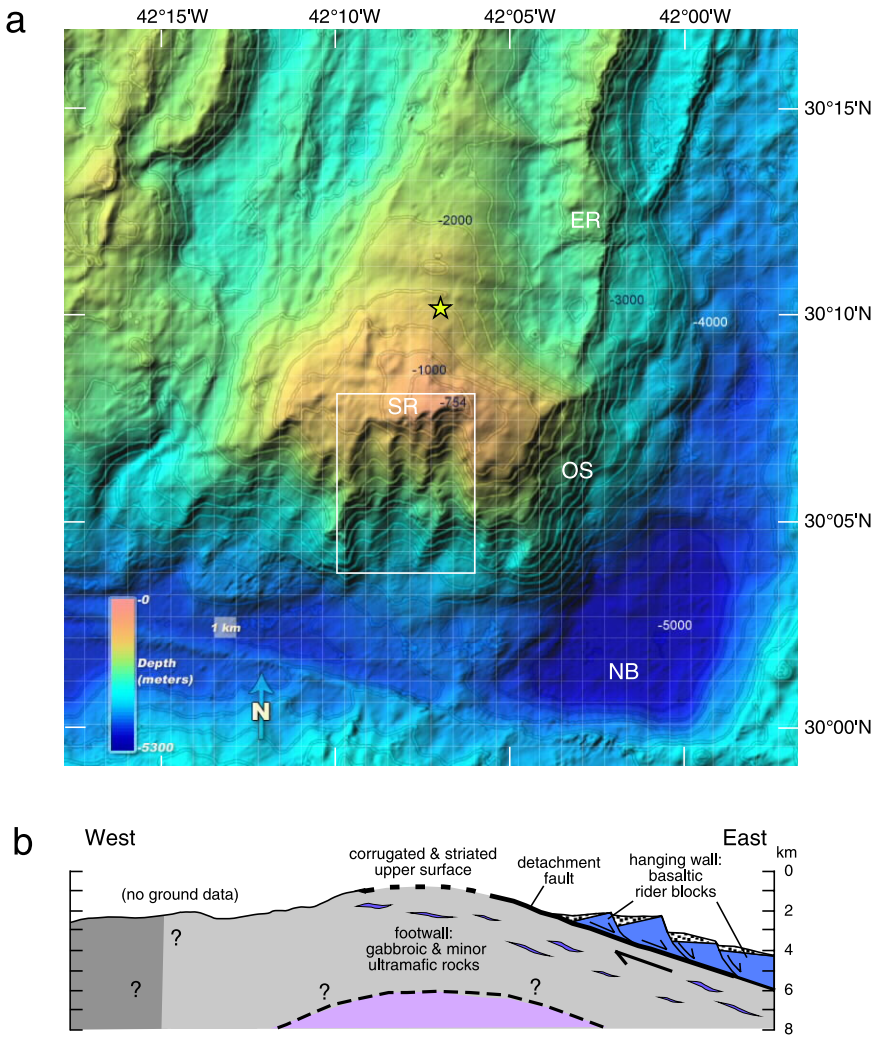

Figure 2. Bathymetry and structure of the Atlantis Massif. (a) Shaded bathymetric map showing the morphology of the Atlantis Massif. The central part of the massif features spreading-parallel corrugations thought to mark a major detachment fault. Star indicates location of IODP Hole 1309D. Box shows location of Figure 3 and study area on the south wall of the massif. Other features referred to in text: ER, eastern ridge, fault-bounded block of basaltic lavas; SR, southern ridge, elevated, transform-parallel ridge sculpted by mass wasting; OS, oblique fault scarp; and NB, nodal basin at ridge-transform intersection [after *Kelley et al.*, 2005]. (b) Schematic cross section across the *central part* of the massif. Faulted, hanging wall, basaltic rocks (blue) are displaced relative to underlying footwall of dominantly gabbroic rocks (gray) and ultramafic rocks (purple) along a major detachment fault (bold line). This interpretation contrasts with results from the *south wall*.

detailed observations and coordinated sampling of a well-defined, continuous, low-angle, detachment shear zone at the top of the south wall of the massif. This study helps put the results of previous and ongoing studies of the Atlantis Massif in a broader tectonic context and invites comparisons with other OCCs.

3. Methods

[11] In this study, we use several different types of data to map the geology of the south wall of the Atlantis Massif. Data from two separate cruises (AT3-60 and AT7-34) are included. Other results from these cruises are published elsewhere [*Kelley et al.*, 2001b, 2005; *Blackman et al.*, 2002; *Schroeder et al.*, 2002; *Früh-Green et al.*, 2003; *Schroeder and John*, 2004; *Boschi et al.*, 2006].

[12] SeaBeam bathymetric data are available for the entire study area (Figure 2) [*Blackman et al.*, 2002]. The entire south wall study area has also been imaged by side-scan sonar. *TOBI* (30 kHz) and higher resolution DSL-120 (120 kHz) back-

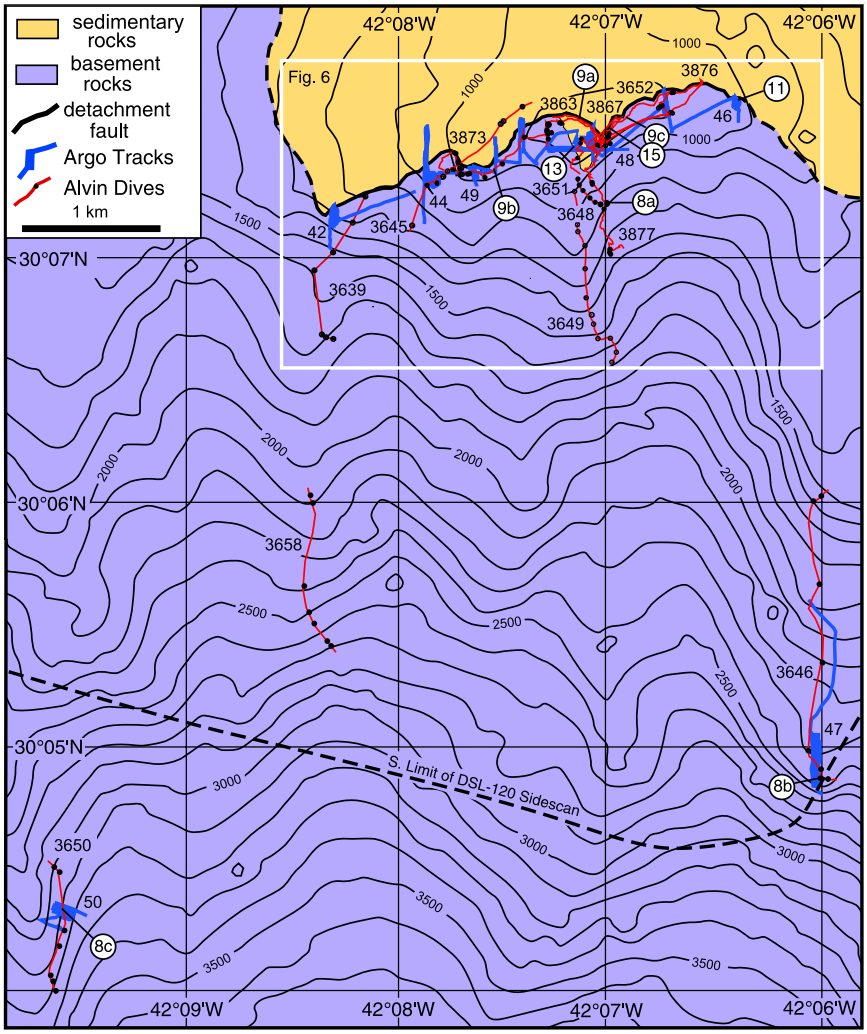

Figure 3. Location map for the south wall of the Atlantis Massif. SeaBeam bathymetry shows the relatively flat top of the massif and the steep south wall. Bold line shows the approximate location of the contact between basement rocks (purple) and overlying sedimentary units (gold) marking a depositional contact over a major detachment fault. *Argo II* ROV transects and mosaic study areas in blue. *Alvin* dive tracks in red with sample locations (black dots; see also Tables 1 and 2). Dense cluster of *Alvin* dives in the center of the area around the Lost City Hydrothermal Field has been omitted for clarity. Entire area north of dashed line is covered by *DSL-120* side-scan sonar imagery. Box shows location of Figure 6. Circled numbers correspond to locations of later figures.

scatter data provide an intermediate-scale context for our near-bottom observations [*Cann et al.*, 1997; *Blackman et al.*, 1998, 2002].

[13] Locations of *Alvin* dives and *Argo II* transects on the south wall are shown in Figure 3. Direct observations and samples were obtained from *Alvin* dives 3639 to 3652 in 2000 and 3862 to 3881 in 2003. Outcrop structures were also mapped using oriented digital images from *Alvin* and the *Argo II* ROV (Lowerings 42 to 50), including individual images (few meters across) and image mosaics (up to several tens of meters across) providing a significantly broader geological perspective. Additional digital images were acquired during NOAA *Argus*/*Hercules* ROV operations near the LCHF in 2005.

[14] Orientations of structures were determined from apparent dips from multiple look-directions. Dip angles from digital images are estimated to be accurate to <5°; strikes to ~10°. Direct measurements with the *Geocompass* [e.g., *Hurst et al.*, 1994] were made periodically and also used to collect oriented samples that could be restored to outcrop orientations.

Table 1. Locations, Water Depths, Lithologies, and Dominant Deformation and Alteration Characteristics of Samples Collected by Submersible in 2003, Atlantis Massif South Wall[a]

Sample	Depth, m	Latitude, N	Longitude, W	Rock Type	Dominant Deformation and Alteration Features	Protolith/Degree of Metasomatism	Comments
3863-1157	862	30°7.506′	42°7.410′	Amphibole fels	Static metasomatism; precursor HT deformation of porphyroclasts; multiple veins	Gb/H	Serp-trem veins (up to 5mm thick); late cc vein cut by pelagic carb vein with microfossils
3863-1204	862	30°7.506′	42°7.410′	Talc-amph schist	Heterogeneous mylonitic texture	UM/H	
3863-1210a	862	30°7.506′	42°7.410′	Amphibole fels	Static metasomatism, precursor HT deformation of porphyroclasts	Gb?/H	Piece 1 of 2
3863-1210b	862	30°7.506′	42°7.410′	Talc-amph schist	Moderate crystal-plastic deformation	UM/H	Piece 2 of 2
3863-1212	862	30°7.506′	42°7.410′	Serpentinite	Local serp ribbon texture and minor fracturing	UM/N-L	Oxidized; late cc veins cut by pelagic carb veins with microfossils
3863-1235	837	30°7.512′	42°7.416′	Talc-amph schist	Strong crystal-plastic deformation	UM/H	Kinked opx; oxidized; late cc veins
3863-1236	837	30°7.512′	42°7.416′	Chlorite-rich rock (blackwall)	Static metasomatism	UM/H	Fe-rich clinochlore (Boschi et al., 2006); late pelagic carb veins
3863-1240	837	30°7.512′	42°7.410′	Talc-amph schist	Strong crystal-plastic deformation; heterogeneous metasomatism	UM/H	Oxidized; chl-rich domains; late cc and pelagic carb veins
3863-1300	834	30°7.512′	42°7.410′	Talc-amph fels	Moderate crystal-plastic deformation; heterogeneous metasomatism	UM/H	Immediately below breccia contact; oxidized; chl-rich domains; late pelagic carb infillings
3863-1301	834	30°7.512′	42°7.410′	Serpentinite	Static serpentinization; precursor HT deformation of opx porphyroclasts; multiple veins	UM/N-L	Immediately below breccia contact; oxidized; serp veins cut by cc/carb veins
3863-1419	794	30°7.542′	42°7.356′	Talc-amph schist (mylonite)	Strong crystal-plastic deformation	UM/H	At breccia contact; relict oxidized serpentinite domains; late cc veins
3863-1425	794	30°7.542′	42°7.356′	Talc-amph schist (mylonite)	Strong crystal-plastic deformation	UM/H	At breccia contact; folded relicts of oxidized serpentinite domains; late cc veins
3863-1526	778	30°7.476′	42°7.140′	Talc-amph schist	Strong crystal-plastic deformation; heterogeneous metasomatism; multiple veins	UM/H	Oxidized serpentinite preserved in center; serp + talc veins cut by late cc veins
3865-1245	795	30°7.452′	42°7.218′	Amph-chl schist (mylonitic)	Strong crystal-plastic deformation; heterogeneous metasomatism	Gb/H	At breccia contact
3865-1355	783	30°7.494′	42°7.128′	Amph schist	Weak foliation defined by amphibole	Gb/H	Porphyroclasts (relict px?); nearly monomineralic
3867-1253	843	30°7.362′	42°7.200′	Mylonitic gabbro	Strong crystal-plastic deformation; dyn rextl; multiple veins	Gb/H	Amph veins, rare plg; preh and zeol veins and cavity fillings

Table 1. (continued)

Sample	Depth, m	Latitude, N	Longitude, W	Rock Type	Dominant Deformation and Alteration Features	Protolith/Degree of Metasomatism	Comments
3867-1254	843	30°7.356′	42°7.200′	Mylonitic gabbro	Strong crystal-plastic deformation; dyn rextl; multiple veins	Gb/H	Preh and zeol veins
3867-1558	748	30°7.488′	42°7.140′	Medium-grained gabbro	Strong crystal-plastic deformation; plg-neoblasts; dyn rextl; heterogeneous metasomatism	Gb/L-M	1.5m below breccia contact; HT brown amph and LT tremolitic amph; chl-rich metasomatic rim
3867-1603	748	30°7.488′	42°7.134′	Medium-grained gabbro	Strong crystal-plastic deformation, plg-neoblast; dyn rextl; heterogeneous metasomatism	Gb/L-M	3.5m below breccia contact; HT brown amph and LT tremolitic amph, chl-rich rim, late pelagic carb vein
3867-1607	751	30°7.494′	42°7.140′	Meta-pyroxenite?	Weak crystal-plastic deformation; local metasomatic domains	UM/N-L	5.5m below breccia contact; px partially to totally replaced by HT brown amph, chl-rich domains
3867-1621	759	30°7.482′	42°7.140′	Serpentinite	Static serpentinization; multiple veins	UM/L	~10m below breccia contact; oxidized; serp + amph±chl veins cut by late cc veins
3867-1623	759	30°7.488′	42°7.140′	Serpentinite	Static serpentinization; heterogeneous metasomatism; multiple veins	UM/L-M	~10m below breccia contact; oxidized; serp + amph±chl veins cut by late cc veins
3869-1126	839	30°7.368′	42°7.194′	Coarse-grained gabbro	Heterogeneous deformation and metasomatism	Gb/L-M	
3869-1220	781	30°7.458′	42°7.182′	Talc-amph schist (mylonitic)	Strong crystal-plastic deformation	UM/H	
3872-1136a	798	30°7.482′	42°7.134′	Serpentinite	Static alteration; multiple veins	UM/H	Serp + amph±chl veins cut by late cc veins
3872-1316	812	30°7.452′	42°7.164′	Serpentinite	Static serpentinization; heterogeneous metasomatism; multiple veins	UM/N-L	Serp veins cut by late cc veins
3872-1350	798	30°7.470′	42°7.146′	Mylonitic gabbro	Weak foliation; incipient rodingitization, multiple veins	Gb/M	HT brown amph, local trem + chl-rich metasomatic domains; preh + chl after plg; preh vein
3873-1124	959	30°7.416′	42°7.842′	Serpentinite/ talc-amph schist	Strong crystal-plastic deformation; localized metasomatism; multiple veins	UM/H	Relict oxidized serpentinite in center; serp + amph±chl veins cut by late cc and pelagic carb veins
3873-1149	958	30°7.386′	42°7.818′	Micro-gabbro	Incipient rodingitization	Gb/M	Chl vein
3873-1216	962	30°7.356′	42°7.806′	Serpentinite/ talc-amph schist	Heterogeneous metasomatism and cataclastic deformation; multiple veins	UM/M-H	Relict oxidized serpentinite with relict ol; serp veins cut by cc veins; carb crust on surface
3873-1245	956	30°7.356′	42°7.806′	Serpentinite	Local cataclastic deformation; heterogeneous metasomatism	UM/M	Oxidized; metasomatic rim; serp + amph±chl veins

Table 1. (continued)

Sample	Depth, m	Latitude, N	Longitude, W	Rock Type	Dominant Deformation and Alteration Features	Protolith/Degree of Metasomatism	Comments
3873-1250	956	30°7.338′	42°7.776′	Amph-rich talc schist (mylonitic)	Strong crystal-plastic deformation	Gb/H	Possibly mixed protolith
3873-1300	950	30°7.338′	42°7.776′	Serpentinite	Moderate crystal-plastic deformation; ribbon textured serp; multiple veins	UM/M	Oxidized; relict ol; metasomatism in local mylonitic domains; serp veins cut by late cc veins
3873-1317	943	30°7.338′	42°7.764′	Serpentinite/ talc-amph schist	Heterogeneous deformation and metasomatism; multiple veins	UM/M	Relict oxidized serpentinite with local cataclastic def; metasomatic domains with moderate crystal-plastic def; serp + amph±chl veins cut by late cc veins
3873-1344	923	30°7.332′	42°7.686′	Mylonitic serpentinite/ talc schist	Heterogeneous crystal-plastic deformation; mylonite and metasomatism in distinct zones	UM/M-H	At contact to sedimentary caprocks; relict serpentinite mylonite with preserved ol; oxidation at contact to metasomatic zones
3873-1413	917	30°7.374′	42°7.614′	Serpentinite	Moderate crystal-plastic deformation; ribbon textured serp; metasomatism in local mylonitic domains	UM/L-M	Precursor HT deformation of opx porphyroclasts; relict ol; serp veins
3873-1544	797	30°7.500′	42°7.392′	Mylonitic metagabbro	Strong crystal-plastic deformation, plg-neoblast, dyn rextl	Gb/N-L	HT brown amph after primary px; originally coarse grained
3873-1548	797	30°7.500′	42°7.392′	Mylonitic metagabbro	Strong crystal-plastic deformation, plg-neoblast, dyn rextl	Gb/N-L	HT brown amph after primary px; originally coarse grained
3876-1117	869	30°7.458′	42°7.122′	Medium-grained gabbro	Minor crystal-plastic deformation	Gb/N-L	HT green amph after primary px; def twin in plg; cut by zeolite veins. Pelagic carb coating on surface
3876-1215	798	30°7.482′	42°7.140′	Coarse-grained pyroxenite	Net-veined	UM/L	HT green amph after px; veins filled with preh + zeol
3876-1310	774	30°7.656′	42°.834′	Serpentinite/ Incipient talc fels	Static serpentinization and metasomatism, microfractures	UM/M	At breccia contact; talc-amph filled microfractures cut by late cc veins
3877-1144	1150	30°7.026′	42°7.116′	Serpentinite (mylonitic)	Heterogeneous crystal-plastic deformation and metasomatism; ribbon textured serp; multiple veins	UM/M	Oxidized; serp + amph±chl veins cut by late cc veins and carb infillings
3877-1158	1115	30°7.026′	42°7.122′	Serpentinite (local metasomatism)	Heterogeneous crystal-plastic deformation and metasomatism, microfractures; multiple veins	UM/L-M	Metasomatism associated with 3 cm thick talc-trem-chl vein, cut by late cc veins
3877-1205	1115	30°7.020′	42°7.122′	Coarse-grained metagabbro	Strong rodingitization, veined	Gb/H	Preh-rich; cc veins

Table 1. (continued)

Sample	Depth, m	Latitude, N	Longitude, W	Rock Type	Dominant Deformation and Alteration Features	Protolith/Degree of Metasomatism	Comments
3877-1307	1017	30°7.218′	42°7.140′	Serpentinite	Ribbon textured serp, microfractures; multiple veins	UM/N-L	Weakly oxidized; serp veins; orthogonal cc vein network
3877-1313	1009	30°7.224′	42°7.140′	Amph-chl fels	Minor crystal plastic deformation; multiple veins	UM/H	Relict oxidized serpeninite domains; relict Cr-spinel; up to 5 cm thick trem-asbestos veins
3877-1344	913	30°7.320′	42°7.206′	Serpentinite	Ribbon textured serp	UM/N-L	Serp veins; in-situ brecciation with pelagic carb infilling
3877-1406	908	30°7.320′	42°7.200′	Serpentinite	Well preserved porphyroclastic texture; ribbon and hourglass serpentine; multiple veins	UM/N-L	Precursor HT def. of opx porphyroclasts; serp veins cut by late cc veins
3879-1253	847	30°7.476′	42°7.170′	Serpentinite	Static metasomatism	UM/N-L	Late cc veins
3880-1349	819	30°7.236′	42°7.086′	Course-grained Fe-Ti gabbro	Plg-neoblast, dyn rextl	Gb/L	Oxide-rich; HT green amph after px; local preh after plg; chl vein
3881-1119	860	30°7.404′	42°7.128′	Serpentinite	Static serpentinization; multiple veins	UM/N	Serp veins cut by late cc veins
3881-1132a	822	30°7.422′	42°7.098′	Serpentinite	Ribbon textured serp; multiple veins	UM/N	Serp veins; minor late cc veins

[a] Mineral abbreviations and textures: amph, amphibole; serp, serpentine; trem, tremolite; chl, chlorite; ol, olivine; plg, plagioclase; px, pyroxene; opx, orthopyroxene; preh, prehnite; zeol, zeolite; cc, calcite; carb, sedimentary carbonate; def, deformation; dyn rextl, dynamic recrystallization mineral fabrics; HT, high temperature (amphibolite-granulate facies); LT, lower temperature (greenschist facies). Rock abbreviations: UM, ultramafic protolith; Gb, gabbroic protolith. Degree of metasomatism reflects the relative modal amounts of the characteristic metasomatic minerals talc, amphibole, chlorite: N, negligible <10%; L, low 10–30%; M, moderate 30–60%; H, >60%.

Table 2. Locations, Water Depths, and Sample Description of Sedimentary Rocks Collected by Submersible in 2003, Atlantis Massif, South Wall and Lost City Areas

Sample	Depth, m	Latitude, N	Longitude, W	Sample Description
				Breccias
3863-1403	799	30°7.536′	42°7.398′	Clast supported, variably rounded, poorly sorted clasts of basalt, up to 20 cm in length.
3865-1250	796	30°7.458′	42°7.224′	Matrix supported; angular to subrounded, poorly sorted clasts of basalt and minor serpentinite/talc schist, up to 10 cm in length.
3867-1116	746	30°7.500′	42°7.146′	Matrix supported (fossil-rich): Variably rounded, poorly sorted clasts of basalt, up to 3 cm in diameter.
3872-1347	798	30°7.470′	42°7.140′	Pelagic carbonate infilling in shear zone with abundant lithic fragments of serpentinite and talc-schist, weak foliation.
3873-1137	943	30°7.422′	42°7.830′	Matrix supported, with multiple carbonate infillings and local cavities; semiangular, poorly sorted clasts of variably altered basalt, up to 10 cm in length.
3873-1343	923	30°7.332′	42°7.686′	Matrix supported; angular, poorly sorted clasts of serpentinite and talc schist up to 3 cm in length; weak foliation. Next to sample 3873-1344.
3873-1440	879	30°7.482′	42°7.518′	Clast supported, poorly lithified, variably rounded, clasts of mylonitic gabbro up to 10 cm in length, fossil-rich matrix with abundant macrofauna (coral dominated).
3880-1201	794	30°7.278′	42°7.122′	Serpentinite breccia; poorly sorted, angular-subangular serpentinite clasts, up to 15 cm long in carbonate matrix with abundant serpentinite debris <1 cm in diameter. Resembles cemented talus debris.
				Sedimentary Carbonates
3862-1549	754	30°7.464′	42°7.158′	Pelagic limestone at top of scarp; well lithified but with cavities; abundant micro- and macrofauna debris and sand-sized lithic fragments.
3863-1811	787	30°7.476′	42°7.152′	Bioclastic limestone; highly porous and with cavities but well lithified, abundant micro- and macrofauna debris, single fossilized corals, multiple sedimentary carbonate generations.
3867-1121	746	30°7.482′	42°7.140′	Chalk, top of scarp; fossil-rich, minor lithic fragments.
3867-1123	746	30°7.488′	42°7.164′	Pelagic limestone at top of scarp; fossil-rich, well lithified with cavities, minor lithic fragments.
3873-1203	962	30°7.356′	42°7.806′	Bioclastic carbonate infilling in basement; inhomogeneous lithification, fossil-rich, sponge-like network of cavities partly filled with soft sediment.
3873-1233	956	30°7.338′	42°7.806′	Bioclastic carbonate infilling in basement; fossil-rich, well lithified, minor lithic fragments, sponge-like porous surface with sediment-filled cavities.
3876-1309	774	30°7.656′	42°6.834′	Foraminifera-rich chalk at top of scarp, semiconsolidated.
3877-1214	1105	30°7.032′	42°7.122′	Foraminifera-rich carbonate infilling in basement; semiconsolidated, serpentinite lithic fragments.

[15] In many cases, strongly foliated intervals and isolated shear zones display kinematic indicators that are used to determine the general sense of movement across these intervals. Geometric constraints are insufficient to determine accurate slip-lines for these displacements, however, our data permit us determine if inclined shear zones have had normal or reverse sense of movement. We use the same general criteria employed in mesoscopic to microscopic structures in continental shear zones that rely on relative displacements determined from asymmetrical fabric elements and minor shear displacements [*Berthe et al.*, 1979; *Simpson and Schmid*, 1983; *Lister and Snoke*, 1984; *Passchier and Simpson*, 1986].

[16] Cut slabs and thin sections of rock samples were used to evaluate outcrop-scale deformation features. Sample locations and descriptions are summarized for basement rocks and sedimentary rocks in Tables 1 and 2, respectively. More detailed descriptions of the rock materials collected during the 2 cruises can be found in other publications [*Schroeder et al.*, 2002; *Früh-Green et al.*, 2003; *Schroeder and John*, 2004; *Boschi et al.*, 2006].

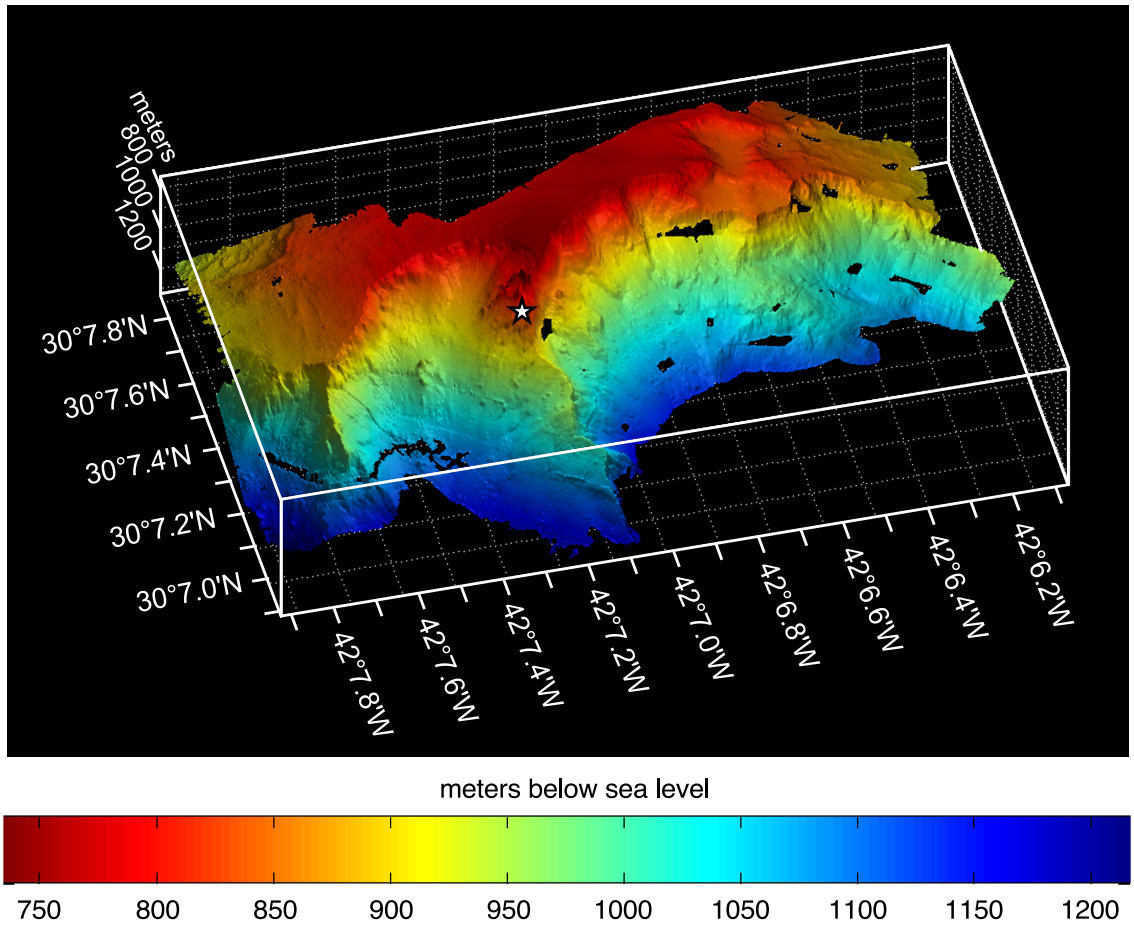

Figure 4. High-resolution bathymetry of the top of the south wall of the Atlantis Massif. Three-dimensional image of the entire ABE SM2000 map area viewed to northeast. Black areas are data gaps. Compare to SeaBeam bathymetry (Figures 2 and 3). Note extremely flat top of the massif and arcuate scarps formed by mass movements. Star shows location of Lost City Hydrothermal Field.

[17] During the 2003 field program, high-resolution (~2 m) bathymetric data were collected with *ABE* in the vicinity of the Lost City Hydrothermal Field (LCHF). Maps and other images were generated by merging the results of numerous transects along and across the top of the massif with varying paths in order to avoid the creation of artifacts (Figure 4). Data were processed with a volumetric surface extraction algorithm [*Curless and Levoy*, 1996]. This perspective reveals an unprecedented level of detail of the fine-scale morphology of the top edge of the Atlantis Massif that we link directly to outcrop geology (Figure 5).

4. Geology of Southern Wall of the Atlantis Massif

[18] The southern edge of the Atlantis Massif is a steep, rugged, series of cliffs exposing a vertical section of as much as 3000 m of the massif (Figures 2 and 3). The top of the massif immediately above the wall is extremely flat and lies at a depth of about 700–800 m. Nearby, this surface has striations similar to those of the central core of the massif about 1000 m deeper and 3 to 10 km to the north (Figure 2a) [*Blackman et al.*, 2002]. Along the southern edge of the massif, mass wasting has created large, arcuate scarps with near-vertical headwalls up to 200 m high (Figures 3 and 4) and substantial talus accumulations. The steep cliffs created by mass wasting provide large, laterally and vertically continuous exposures that reveal a cross section of the internal structure of this OCC.

[19] In the following sections we describe the morphology, lithologies and outcrop structures of the basement and sedimentary cover rocks exposed on the south wall. The structures in the basement

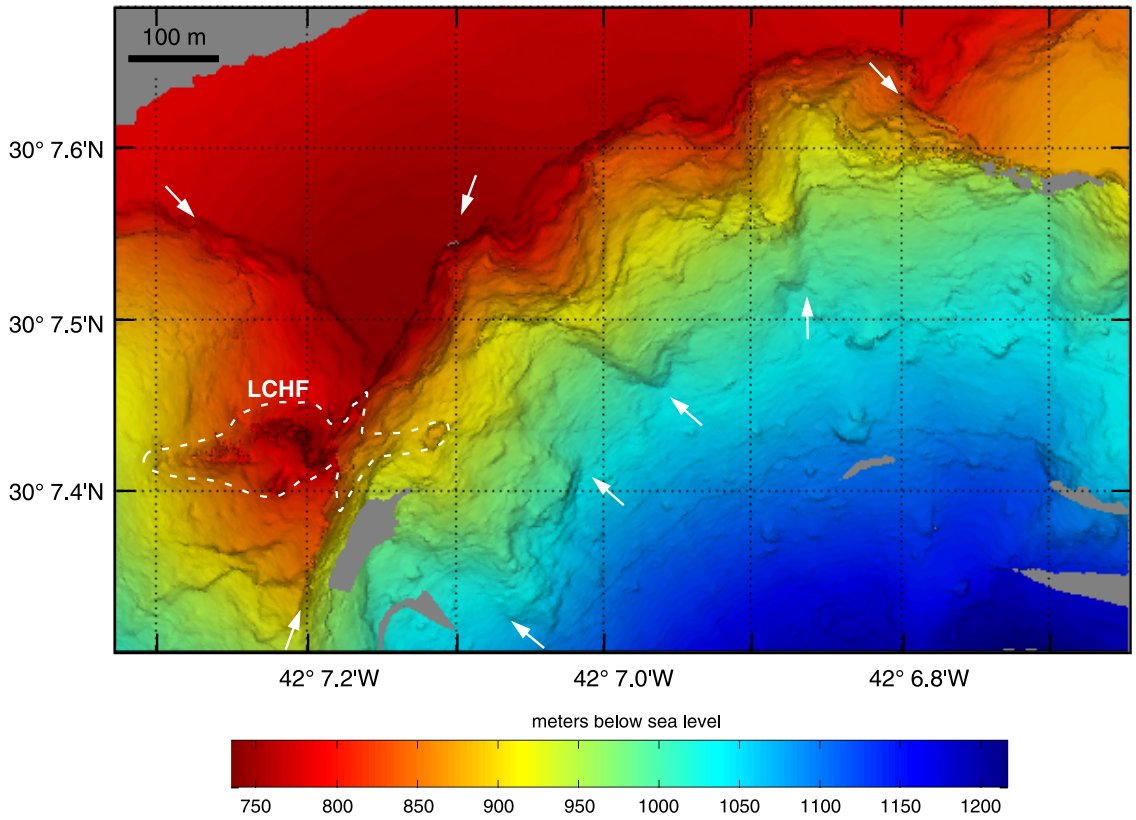

Figure 5. High-resolution bathymetric image of part of the south wall of the Atlantis Massif generated from ABE SM2000 bathymetry and processed with a volumetric surface extraction algorithm [*Curless and Levoy*, 1996]. Upper 100 m of scarp has distinctive horizontal ledges corresponding to outcrops of the DSZ. Note steep scarps of normal faults (white arrows) that control mass wasting where they intersect the top of the massif. These faults offset the DSZ and displace the terrace where the LCHF is situated. The faults do not affect the flat upper surface of the massif. LCHF, Lost City Hydrothermal Field. White dashed line, limit of hydrothermal field. See text for further explanation.

rocks include (1) igneous and high-temperature deformation structures in massive rocks typical of the bulk of the material exposed on the south wall, (2) a continuous, intensely deformed detachment shear zone near the top of the wall, (3) a family of crosscutting ductile shear zones, and (4) steeply dipping normal faults that cut all the other basement structures. Sedimentary rock units that directly overlie the basement rocks postdate all but the latest normal faults. They include a diverse suite of sedimentary breccias and overlying pelagic limestones. We summarize these results in the form of a geological map and cross section (Figures 6 and 7) of this key portion of the Atlantis Massif. Descriptions of the lithologies and structures in this area are followed by our interpretations. The relationships among these features and how they may relate to the evolution of this OCC are discussed in a later section.

4.1. Massive Ultramafic and Mafic Rocks

[20] Extensive exposures of basement rocks on the south wall include variably deformed and metamorphosed ultramafic and lesser mafic rocks [*Blackman et al.*, 2002; *Boschi et al.*, 2004, 2006; *Schroeder and John*, 2004]. On the basis of the collections made during both the 2000 and 2003 investigations, approximately 70% of the samples collected by submersible in this area are variably altered ultramafic rocks derived from harzburgitic protoliths (Table 1), typical of residual upper mantle material [e.g., *Dick*, 1989]. Metagabbros and possible metapyroxenites make up the remaining 30% of the samples (Table 1). In some cases these are so intensely altered that their protoliths cannot be unambiguously determined [*Boschi et al.*, 2006]. This lithological assemblage is notably different from the gabbro-dominated core recovered just 5 km to the north at IODP

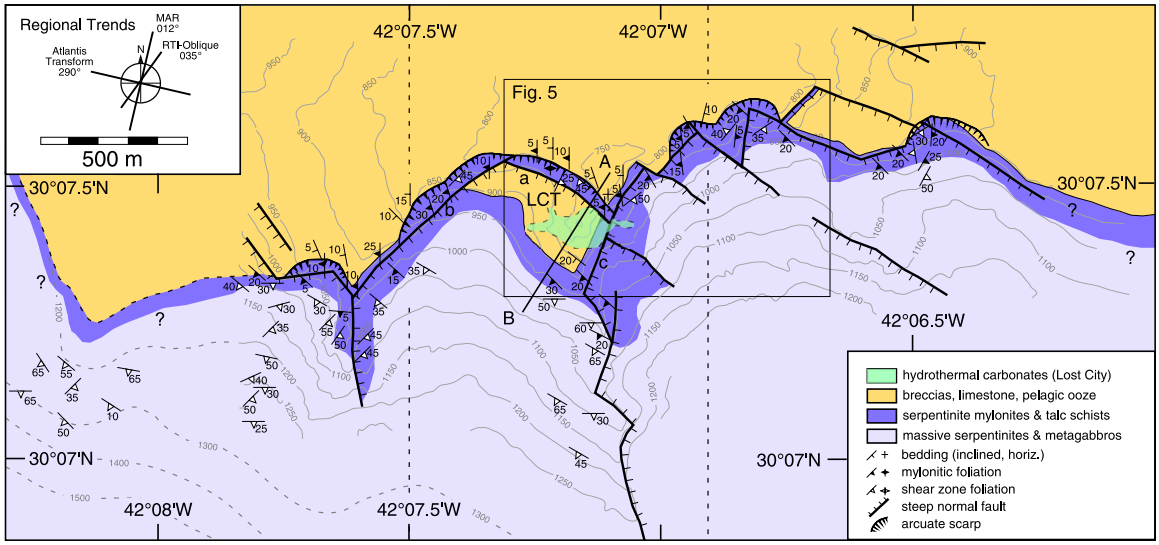

Figure 6. Geologic map of the top of the south wall of the Atlantis Massif. The DSZ (dark purple), defined by strongly schistose and mylonitic rocks, lies above massive, jointed basement exposures (light purple). The mylonitic shear zone foliation (closed symbols) roughly parallels the top of the massif. Later, isolated shear zones (open symbols) and steep normal faults cut the mylonitic foliation. The DSZ is unconformably overlain by undeformed sedimentary rocks (breccias and limestones) and unconsolidated pelagic ooze (gold). Mass wasting has created steep, arcuate escarpments at the top of the south wall that are localized along inactive, steeply dipping normal faults. These faults do not cut the sedimentary units, which were deposited after faulting. The Lost City Hydrothermal Field (green) is situated on the Lost City Terrace (LCT), a down-dropped block (bounded by faults a, b, and c) on the edge of the wall. Inset shows regional trends of the MAR, Atlantis Transform Fault, and a major oblique fault scarp at the RTI. A-B indicates location of cross section in Figure 7. Box shows location of Figure 5. Map extends about 500 m west of area shown in Figure 4.

Hole U1309D where dominantly gabbroic rocks were recovered.

[21] Outcrops of serpentinized peridotite in this area have a massive, sparsely jointed (Figures 8a and 8b) to knobby appearance. Joint patterns are generally planar and mainly nonsystematic. Some outcrops show systematic, even joint spacing, locally in orthogonal joint sets. Although outcrops typically lack obvious mesoscopic deformation features, samples show that the peridotites retain porphyroclastic textures probably acquired during high-temperature deformation and recrystallization in the mantle (Table 1). Mesh-textured serpentine with well-preserved kernel textures and variable densities of crosscutting serpentine veins (Figure 8c) indicate essentially static overgrowth by lower temperature, hydrous minerals [*Schroeder and John*, 2004; *Boschi et al.*, 2006].

[22] Outcrops of mafic material tend to have very massive, smooth surfaces and widely spaced, planar, systematic joint patterns. There appear to be many relatively small-scale (tens of meters) bodies of gabbroic material, but details of shape, size, and contacts of these gabbro bodies could not be determined.

[23] Samples of mafic rocks show a broad range of deformational and metasomatic effects [*Boschi et al.*, 2004, 2006; *Schroeder and John*, 2004]. Igneous textures are commonly overprinted by crystal-plastic deformation including granulite to

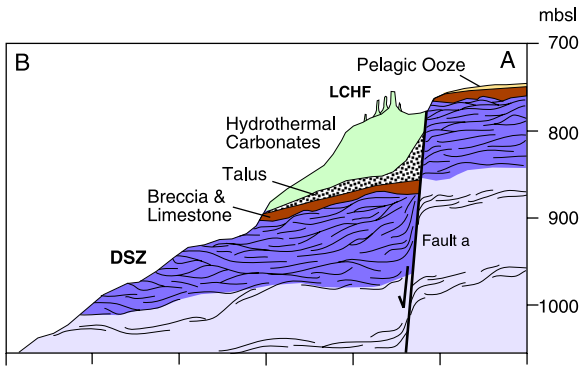

Figure 7. Cross section of the Lost City Terrace. Section line A-B trends northeast-southwest and crosses the LCHF. The top of the DSZ has at least 100 m vertical separation across northwest trending normal fault a (Figure 6).

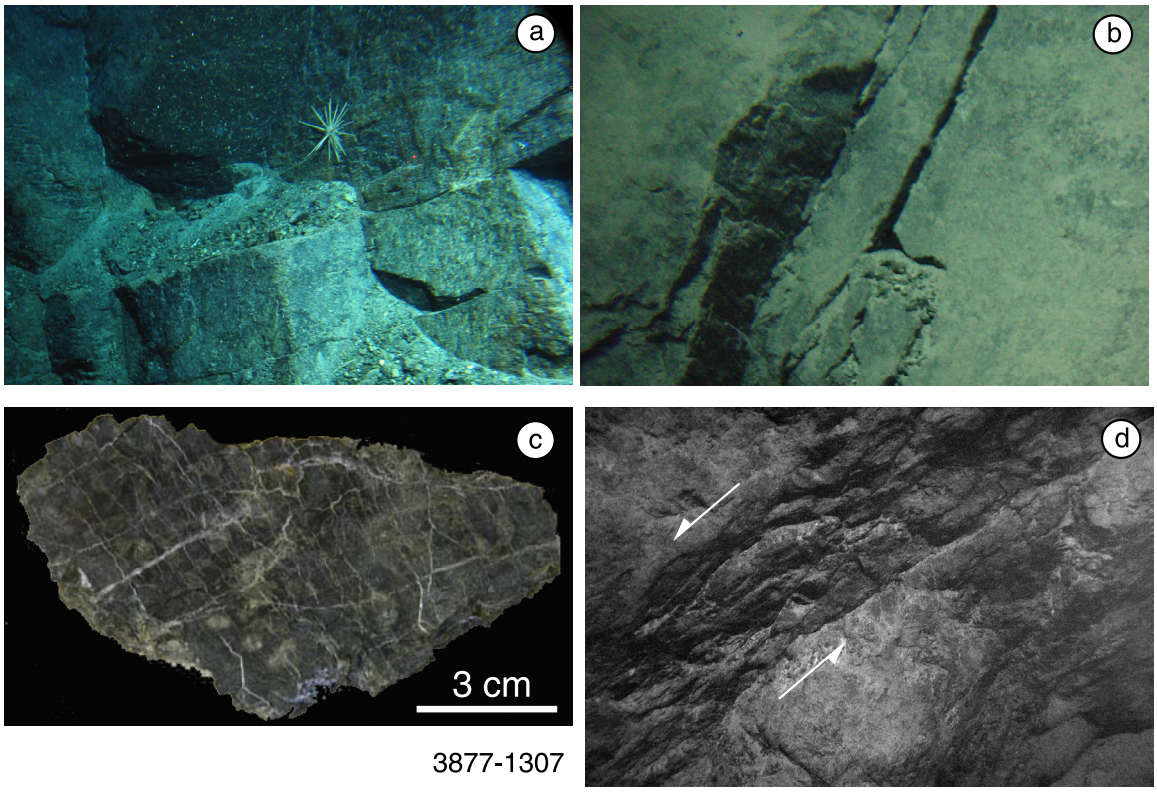

Figure 8. Basement rocks below the DSZ. (a) Massive, jointed, serpentinized peridotite about 200 m below the DSZ from *Alvin* Dive 3877 (1168 m). (b) Fractured massive rock (metagabbro?) from *Alvin* 3646 (2480 m). (c) *Alvin* sample 3877–1307, a serpentinized peridotite with calcite veins from outcrops near Figure 8a. (d) Shear zone in massive basement rock, asymmetrical fabric indicates normal displacement (half-arrows), view to N, Argo 50 (3100 m). Horizontal dimensions of outcrops are ~2 m in Figures 8a and 8b and 5 m in Figure 8d.

amphibolite facies mylonites. Narrow cataclastic bands with greenschist facies assemblages cut the higher temperature assemblages. Rare dikes are characterized by continuous, roughly planar joints bounding slabs with evenly spaced cross-joints [*Blackman et al.*, 2002].

[24] In this part of the basement exposures, high-temperature deformation began at anhydrous conditions resulting in crystal-plastic deformation and recrystallization of both peridotites and gabbroic rocks under low-pressure, granulite facies conditions. This deformation appears to have affected virtually all of the ultramafic rocks and most of the mafic rocks of the south wall. Some gabbro bodies are not deformed and retain igneous textures suggesting that they were intruded after most of this deformation; others are mylonitic (Table 1). Local shear zones developed at relatively high-temperature, hydrous (amphibolite facies) conditions [*Schroeder and John*, 2004]. Although low-temperature, static replacement of higher temperature phases (e.g., serpentinization) is widespread in the south wall rocks, deformation during serpentinization appears to have been limited to widely spaced shear zones. All samples from *Alvin* dives and *Argo II* transects below about 1150 m are composed mainly of these massive materials (Figure 3). Locally, the massive rocks are cut by strongly foliated shear zones ranging from a few centimeters to 2 m wide (Figure 7d). Samples from these intervals show evidence of crystal plastic deformation overprinted by lower temperature serpentinization. The shear zones and distinctive, steeply dipping fault zones (see below) contrast strongly with the relatively undeformed appearance of most of outcrops in the lower part of the south wall.

4.2. Detachment Shear Zone

[25] Near the top of the south wall (above about 1150 m) the appearance of outcrops contrasts strongly with those of the deeper basement rocks. The massive material grades rapidly upward into outcrops with a strong mesoscopic foliation that

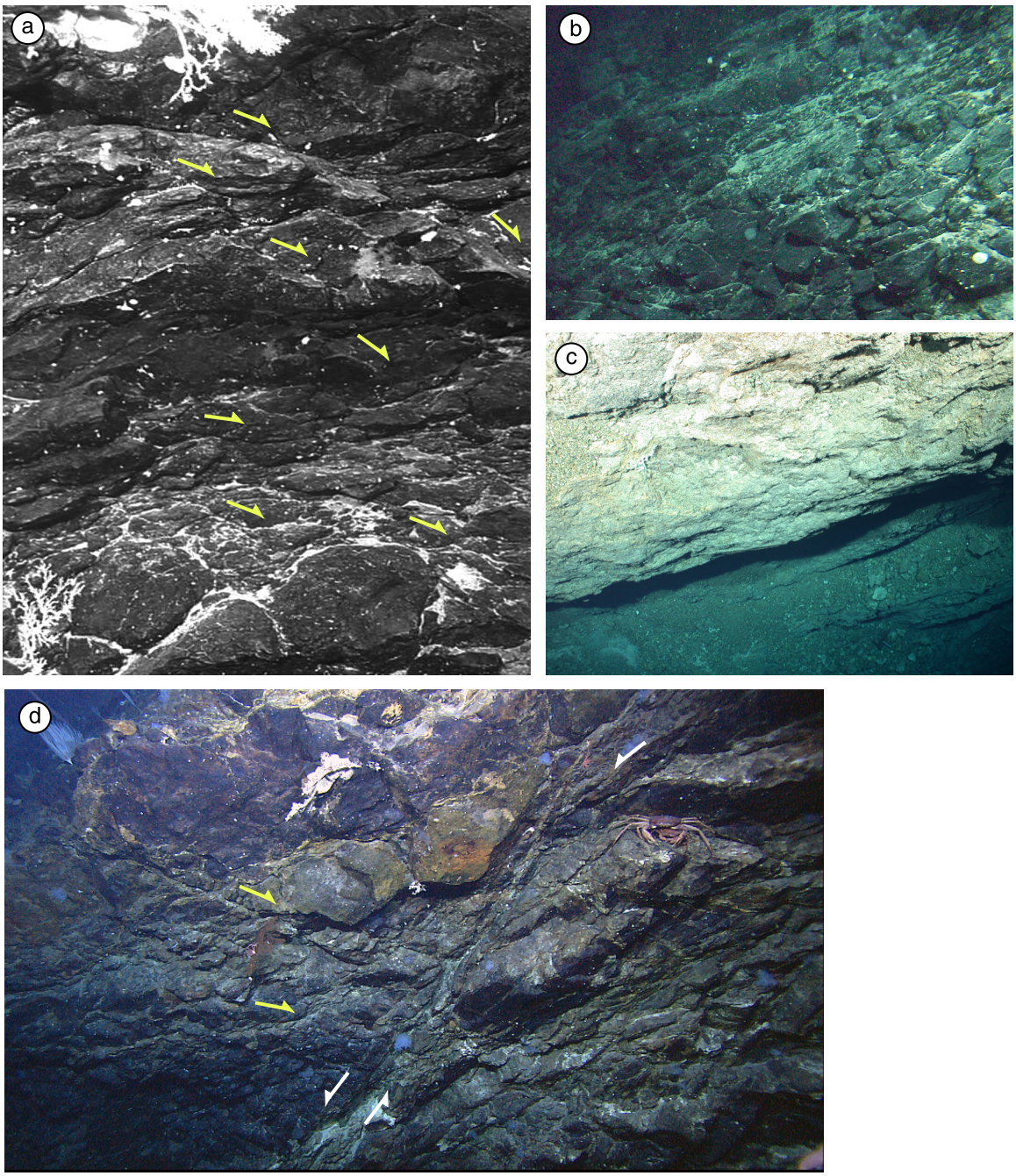

Figure 9. Outcrop images of the DSZ. (a) Mylonitic serpentinite, half-arrows show top-to-E (normal) sense of slip on shear zones, *Alvin* digital image mosaic, *Alvin* 3863 (793 m). (b) Planar to phaccoidal foliation in mylonitic serpentinite dips gently to the west in the central to western parts of the study area, *Alvin* 3873 (956 m). (c) Finely laminated mylonitic serpentinite and talc-amphibole schists forming prominent horizontal ledges, *Alvin* 3867 (811 m). (d) Phaccoidal serpentinite with typical anastomosing fabric in the DSZ 200 m northeast of the LCHF. Mylonitic fabric is near horizontal with top-to-E displacement (yellow half-arrows). Later west-dipping shear zone cuts the mylonitic fabric and has normal slip displacement (white half-arrows). *Hercules* digital image. Horizontal dimensions of Figures 9a–9c are about 2 m, and dimensions of Figure 9d are about 3 m. (Image from University of Washington, NOAA, IFE, and University of Rhode Island, IAO).

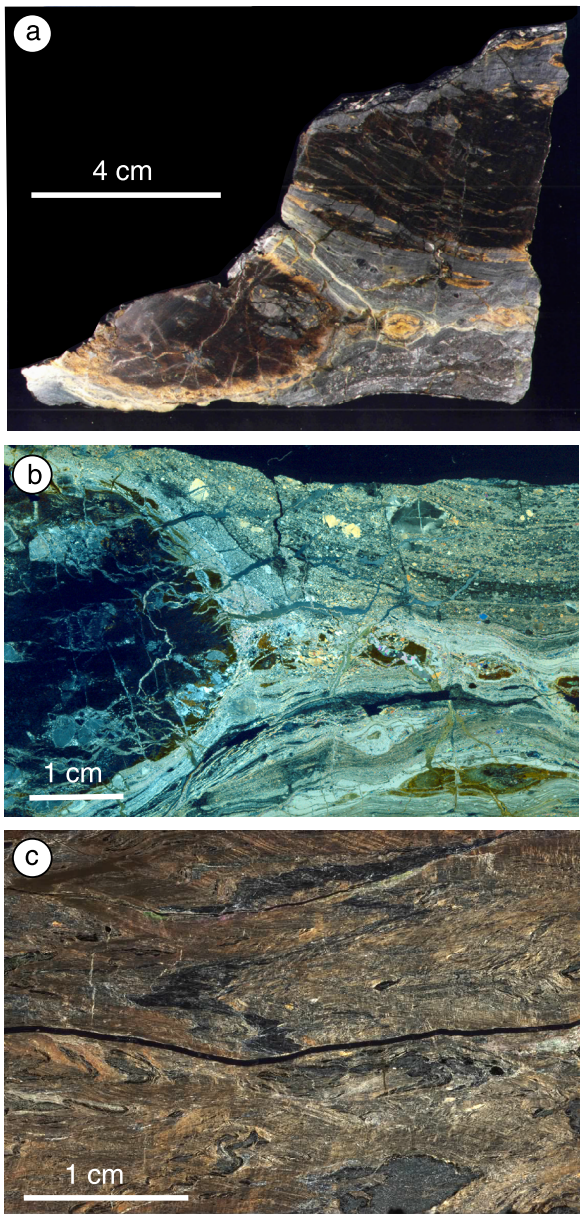

Figure 10. Deformation fabrics in intensely deformed rocks from the DSZ. (a) Cut slab of phaccoidal shear zone rock. Dark lenses of serpentinized porphyroclastic peridotite (lower left) and mylonitic serpentinite (upper right) are separated by light-colored, anastomosing bands of fine-grained, talc-tremolite schist. *Alvin* sample 3873–1344 (922 m). (b) Photomicrograph of lower portion of sample shown in Figure 10a. (c) Photomicrograph of mylonitic serpentinite-talc-amphibole schist with complexly folded mylonitic fabric. *Alvin* sample 3863–1425 (793 m). See Table 1 for sample locations.

can be traced in a continuous unit across the top of the massif (Figure 6) and that we identify as a detachment shear zone (DSZ). Rocks in this interval have a platy character with lenses and discontinuous sheets of relatively massive material a few centimeters to a few meters thick surrounded by shear zones with anastomosing to laminated foliations (Figures 9–11). In some places, this deformation fabric is pervasive over vertical outcrop intervals of at least several meters. Dense sampling on several dives recovered schistose and mylonitic rocks from these shear zones (Figure 10). Mylonitic fabrics commonly cut and deform preexisting deformation fabrics in the DSZ attesting to its protracted history of displacement and large bulk strains. The shear zone rocks feature discontinuous, lensoid, bands of dark, serpentinite and lighter colored talc + Ca-amphibole schists and show highly variable textures indicative of strain localization in the domains of most highly altered material [*Früh-Green et al.*, 2002; *Boschi et al.*, 2003; *Schroeder and John*, 2004]. Metasomatic alteration of the basement rocks to talc-bearing assemblages is a key aspect of the DSZ and is similar to alteration along detachment faults in other OCCs, such as at 15°45′N [*Escartín et al.*, 2003]. Metasomatism is associated with varying degrees of ductile to brittle deformation under greenschist-facies conditions and suggests that Si-rich fluids were channeled along foliation surfaces and fractures during the evolution of the OCC [*Boschi et al.*, 2003, 2006]. In the ultramafic rocks, serpentine textures are locally overgrown by talc-amphibole-chlorite assemblages that are in turn cut by later serpentine and/or calcite veins [*Schroeder and John*, 2004; *Boschi et al.*, 2006]. In a previous study, *Schroeder and John* [2004] suggested that the intensity of cataclastic deformation increased upward toward the top of the south wall. Subsequent detailed sampling across the DSZ documents that rocks from this area have mainly crystal-plastic deformation (Table 1) [*Boschi et al.*, 2006]. Although these rocks are highly altered, protoliths appear to have about the same proportion of ultramafic to mafic material as in the underlying massive rocks, suggesting that the DSZ developed in similar material.

[26] In general, the intensity of the mesoscopic deformation fabrics increases in intensity upward toward the top of the scarp. The strongly anisotropic fabric of the rock is evident on all scales. Cliff exposures are marked by subhorizontal ledges created by preferential degradation of weaker, less resistant material. The ledges of more resistant material are typically one to several meters thick and are continuous for many meters laterally along the scarp faces. The vertical extent of this strongly

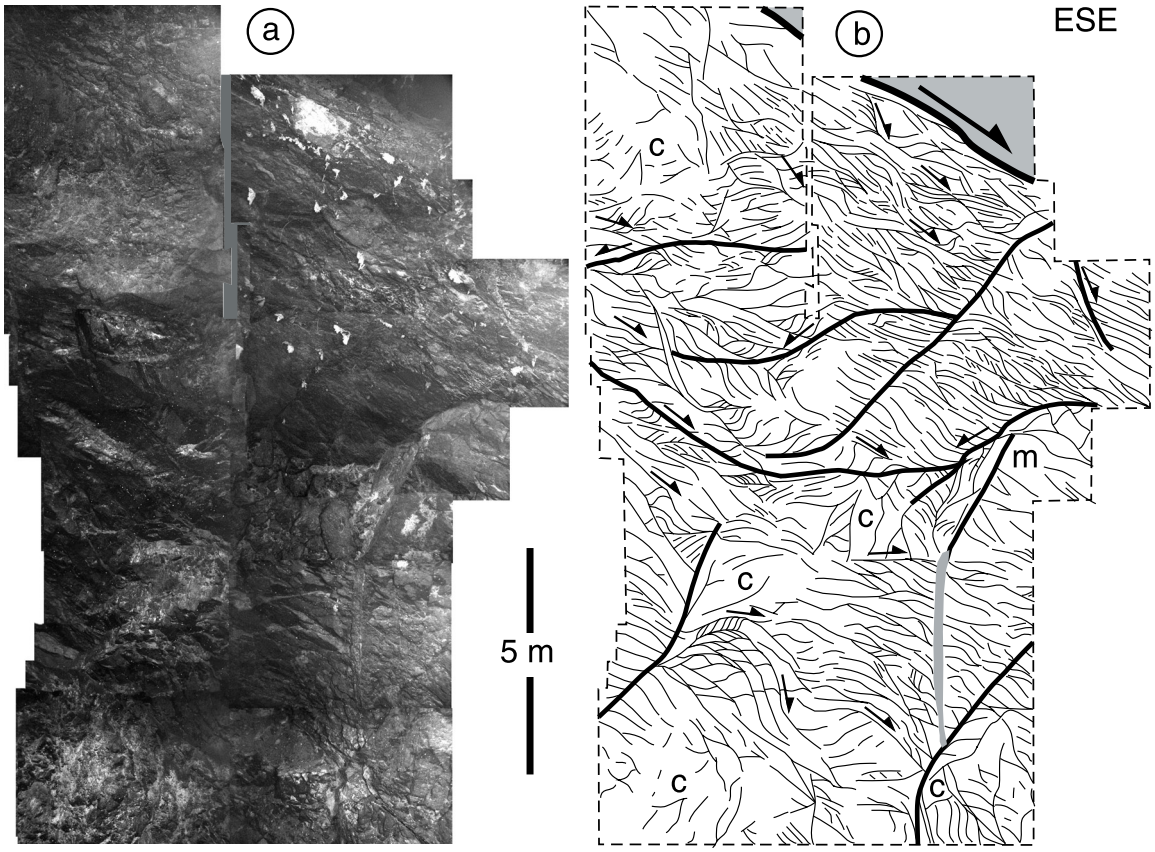

Figure 11. Complex deformation in the DSZ. The DSZ is marked by intensely deformed serpentinites and talc-amphibole schists in variably foliated, lensoid domains separated by more continuous anastomosing shear zones: m, relatively massive material; c, knobby, cataclastic material. Light, vertical streak is a hydrothermal stain. (a) *Argo II* 46 mosaic (915 m). (b) Interpretation. Gray area to upper right is the E-sloping top of the massif covered by pelagic ooze. Overlying sedimentary units have been removed by mass wasting at this site. Note that foliation dips east in this easternmost part of the study area.

foliated interval, based on direct observations from *Alvin* and *Argo II* transects, is about 100 m.

[27] The DSZ shows up in the high-resolution *ABE* bathymetry (Figure 5) as a laterally continuous band of closely spaced, subhorizontal ledges. Less continuous ledges persist down to at least 1000 m depth and deeper where normal fault displacements have occurred. Digital imagery, direct observations, and sampling across this depth interval confirm that this distinctive bathymetric fabric corresponds to a major shear zone composed of mylonitic to strongly foliated serpentinites, talc schists, and lesser metagabbros [*Früh-Green et al.*, 2002; *Boschi et al.*, 2003, 2006; *Schroeder and John*, 2004].

[28] The DSZ is mapped for at least 3 km along the crest of the massif (Figure 6). From its trace across the complex bathymetry of the south wall of the massif, the DSZ and has a gently arched form as it crosses the top of the massif (Figure 6). The internal fabric of the shear zone is more complex with domains of variably sheared material bounded by intensely foliated anastomosing shear zones (Figure 9). To the west, the shear zone fabric dips gently to the west or southwest and reaches a depth of over 1100 m. Near the center of the massif, near the LCHF, the shear zone fabric is subhorizontal to gently west or southwest dipping and is mostly above 950 m depth. Toward the eastern limit of its exposure, the shear zone fabric is more complex with the pervasive, anastomosing fabric cut by gently to moderately east- to southeast-dipping shear zones (Figure 11). Relationships in this area suggest that the DSZ may be cut by a younger shear zone that dips more steeply to the east or southeast. This shear zone may form the major oblique fault scarp that marks the eastern edge of

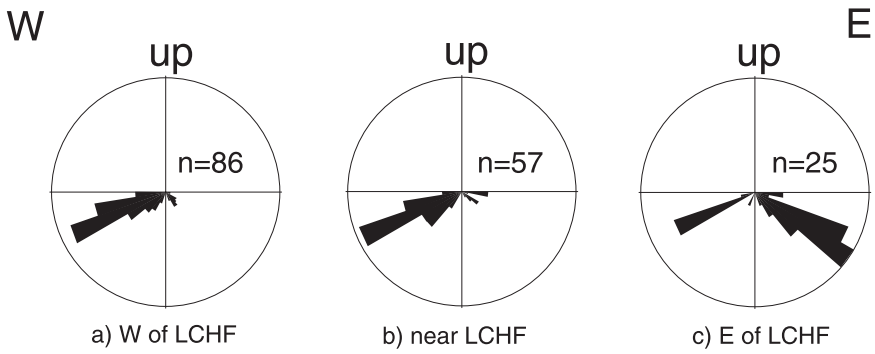

Figure 12. Rose diagrams showing variations in dip of mylonitic foliation in the DSZ across the crest of the south wall. Diagrams are oriented vertically; radius is 30%. (a) Area west of LCHF, (b) area near LCHF, and (c) area east of LCHF. Boundaries between areas indicated in Figures 12a–12c are shown as dashed lines in Figure 6. Foliation dips gently to the west or southwest in the central and western parts of the study area but dips to the east or southeast in easternmost part.

the massif (Figure 2a). The three-dimensional character of the south wall shows that the foliation is horizontal or dips gently (~5°) to the west in the most deeply embayed (most northerly) exposures (Figure 12); however, the foliation dips gently to moderately to the south on major promontories, defining a partial dome-like form.

[29] Kinematic indicators including asymmetrical foliation patterns and porphyroclasts visible in outcrop images and samples (Figures 9–11), indicate a general top-to-east (toward the spreading axis) or -southeast (toward the transform) displacement throughout the DSZ. Even in areas of west-dipping foliation, the sense of displacement in the main shear zone fabric indicates top-to-east movement. These areas might suggest thrust faulting if viewed in isolation. The foliation patterns are locally modified by later shear zones and normal faults as discussed below.

[30] The DSZ contrasts strongly with the underlying basement terrane in terms of its fine-scale outcrop morphology, mesoscopic structures, and rock types. Collectively, the outcrop structures and samples from the DSZ document a history of intense deformation that progressed from amphibolite to greenschist facies conditions in a relatively narrow (~100 m) normal-slip shear zone. The large, noncoaxial strain that affected the DSZ was accompanied by progressive hydrous alteration (serpentinization and metasomatism) under decreasing temperature conditions. This intense, focused retrograde deformation contrasts strongly with the underlying massive basement rocks. The range of rock types collected in the DSZ is similar to that recovered from some other OCCs [*Karson and Dick*, 1983; *Dick et al.*, 2000; *MacLeod et al.*, 2002; *Escartín et al.*, 2003].

[31] Displacement on the order of several kilometers is implied by the dimension of the fault zone in the tectonic transport direction (~3 km; east-west, parallel to corrugations and striations) suggesting at least this much displacement. The dimension parallel to the large-scale corrugation and striation patterns found in bathymetry and backscatter images [*Cann et al.*, 1997; *Blackman et al.*, 2001, 2002] is even greater, about 10 km. The 100-m-thick shear zone, with intensely sheared mylonitic rocks, is consistent with such large displacements. At present we are unable to accurately quantify the shear strain (or displacement) across the DSZ. Even if this were possible, the original thickness of the DSZ is not known and thus limits an accurate calculation of displacement [e.g., *Ramsay and Graham*, 1970]. The lack of a distinct cataclastic fault zone (or microbreccia) at the top of the DSZ may suggest that some of it has been excised by slip on low-angle fault zones or removed by mass wasting.

4.3. Ductile Shear Zones

[32] Discrete shear zones with anastomosing fabrics cut both the massive basement rocks and the DSZ (Figure 9d). These shear zones are typically 10 cm to 3 m wide and can be traced for several meters across outcrop images. Most of them are curviplanar with gently undulating traces. The amount of displacement across these shear zones is not known because of the general lack of appropriate markers. They commonly juxtapose volumes of rock with different joint or foliation patterns. In some places they cut or merge with

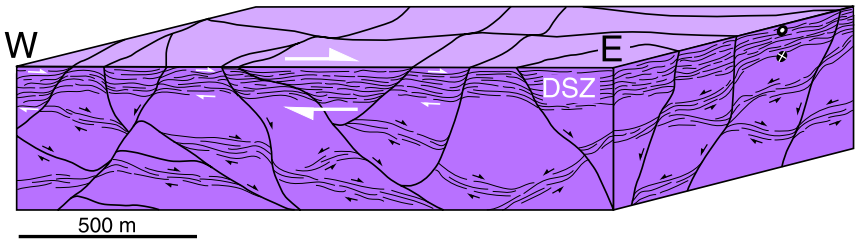

Figure 13. Schematic block diagram summarizing relations in basement rocks of the south wall of the Atlantis Massif. Strongly foliated to mylonitic rocks with medium- to low-temperature deformation fabrics (fine lines) of the DSZ and isolated shear zones deeper in the footwall domain are cut by more continuous, discrete faults and shear zones (bold lines) dipping to the east, west, and south. Kinematic indicators show top-to-east displacement and large noncoaxial shear strain in the DSZ. Normal (oblique?)-slip displacements on the steeper faults and shear zones collectively result in a coaxial, essentially vertical flattening strain. Arching of the DSZ and latest faults not shown.

similar-looking shear zones. In the massive basement rock deeper on the south wall they occur as isolated bands of strongly foliated materials. In the DSZ, the shear zones commonly cut the more pervasive shear zone foliation at moderate to low angles and locally bend to merge into parallelism with it (Figure 11) making it difficult to differentiate these deformation structures on a local scale. Samples of these shear zones show mixed crystal-plastic to cataclastic fabrics dominated by greenschist facies assemblages [*Schroeder and John*, 2004; *Boschi et al.*, 2006].

[33] Direct observations and photogeology show that these shear zones do not have a strong preferred orientation. They tend to dip gently to moderately to the east and west (Figure 6). More sharply defined, steeply dipping shear zones tend to cut the lower angle shear zones. Asymmetric fabrics and minor shear displacements provide kinematic indicators in these shear zones and show evidence of at least a component of downdip (normal) hanging wall displacement in nearly all cases. Oblique displacements cannot be ruled-out with the available data.

[34] The shear zones overprint high-temperature deformation fabrics in the massive basement rocks beneath and within the DSZ. Movement on them overlapped in time with or postdated the slip on the DSZ based on their similar mineralogy and local parallelism. Unlike the DSZ, where a more uniform-sense, top-to-east displacement dominates, movements in the ductile shear zones are persistently downdip (normal) on surfaces dipping in many different directions. Overall, the orientations and kinematic indicators of the ductile shear zones suggest that they accommodated a coaxial strain with a general vertical flattening of the massif (Figure 13).

4.4. Steeply Dipping Normal Faults

[35] Strong lineaments in the bathymetry (Figures 4 and 5) were investigated with *Alvin* and documented as major, steeply dipping normal faults (Figure 6). Outcrop observations and digital image mosaics (Figure 14) show that they truncate the foliated shear zones and joint sets in adjacent masses of rock. In most cases it is not possible to quantify displacements because of a lack of suitable markers. In some cases, faults juxtapose volumes of rock with distinctly different mesoscopic fabrics indicating displacements of at least a few meters (Figure 14). These faults strike mostly northeast and northwest. The northwest-trending faults roughly parallel the regional trend of the Atlantis Transform and may be related to uplift along the transform edge of the massif. The northeast-trending faults may have originated as oblique faults, similar to those found at the MAR-Atlantis ridge-transform intersection (RTI) [*Cann et al.*, 1997; *Blackman et al.*, 2001] and many other RTIs. *Alvin* and *Argo II* images reveal several dip-slope walls of fault breccia with shingled structures. These dip steeply to the south or south-southeast and are probably also relatively late faults. Mass wasting has degraded these faults so that they are not obvious even with fine-scale ABE bathymetry or side-scan sonar.

[36] Several of the steep fault zones were examined in detail in the vicinity of the LCHF. At least 3 major faults bound the Lost City Terrace, a roughly triangular block about 500 m long near the top of the south wall. The LCHF is situated on top of this block. On the north side of the terrace, displace-

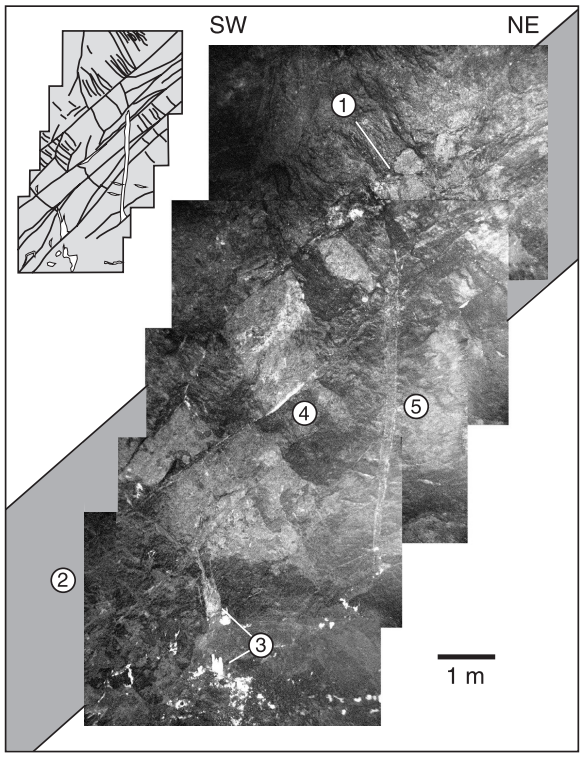

Figure 14. Steeply dipping normal (to oblique) slip fault zone. Relatively sharply defined fault zones cut the DSZ and other shear zones. Here, strongly foliated material of the hanging wall is juxtaposed with massive material in the footwall. This fault and others have channeled hydrothermal fluids near the LCHF. Note: (1) moderately ENE-dipping shear zone with planar foliation (white line); (2) fault zone is about 3 m wide; (3) small carbonate spires mark sites of hydrothermal outflow; (4) white carbonate vein in fault zone; and (5) vertical band of carbonate precipitates on outcrop deposited by leaking hydrothermal fluids. *Argo II* 48 mosaic (882 m). Inset shows interpretation.

ment on a distinct normal fault (Fault *a* in Figure 6) has offset the DSZ and overlying sedimentary units by several tens of meters vertically (Figures 6 and 7). Bedding in the sedimentary rocks on the Lost City Terrace dips gently to the south indicating only minor rotation due to faulting.

[37] The steep normal faults are the latest deformation structures and therefore have likely developed in response to the uplift of the massif. Displacements on them must have postdated movement on the DSZ and the later shear zones, but predated the formation of the smooth upper surface of the massif described below.

[38] Steep faults like those bounding the Lost City Terrace localize the outflow of hydrothermal fluids generated by active serpentinization reactions in the subsurface that have created the LCHF at the crest of the massif [*Kelley et al.*, 2001b, 2005; *Früh-Green et al.*, 2003]. One major northeast-trending fault, just east of the LCHF (Fault *c* in Figure 6) has exposed a stockwork of extensive carbonate net veins similar to ophicalcites found in some ophiolites complexes [e.g., *Treves and Harper*, 1994]. Hydrothermal fluids related to active serpentinization are actively venting along this wall [*Kelley et al.*, 2005].

[39] Although they are no longer active, some of the steep normal faults continue to provide permeable pathways for the ongoing hydrothermal outflow. Volume increases associated with serpentinization and expansion permitted by unloading and mass wasting probably sustain these faults as permeable pathways for hydrothermal flow.

[40] Despite their documented displacements, some of the steeply dipping normal faults cannot be traced northward across the top of the massif (Figures 2 and 4). Therefore significant vertical movement on most of these faults must predate the deposition sedimentary rocks that create the smooth upper surface of the massif.

[41] Many of the steep faults are clearly associated with the arcuate headwall scarps created by mass wasting. The traces of the scarps can be traced downslope for hundreds of meter below the top of the south wall and therefore do not appear to be only surficial features. These faults appear to localize mass wasting where they intersect the DSZ and overlying sedimentary rock units. Serpentinization localized in the DSZ and in the steep faults may have weakened the basement rocks and helped to further localize mass wasting. Alternatively, it is possible that some of these faults may essentially mark the edges of large-scale slide blocks.

4.5. Sedimentary Rock Units

[42] The top of the south wall is marked by a thin (<3 m) section of distinctive sedimentary rocks [*Kelley et al.*, 2001a, 2005; *Schroeder et al.*, 2002; *Früh-Green et al.*, 2003] that directly overlie the DSZ (Figure 15), locally across a gentle angular unconformity. This contact has been traced across the full length of the south wall study area. Locally, the overlying sedimentary unit has been broken into blocks up to a few meters across that are

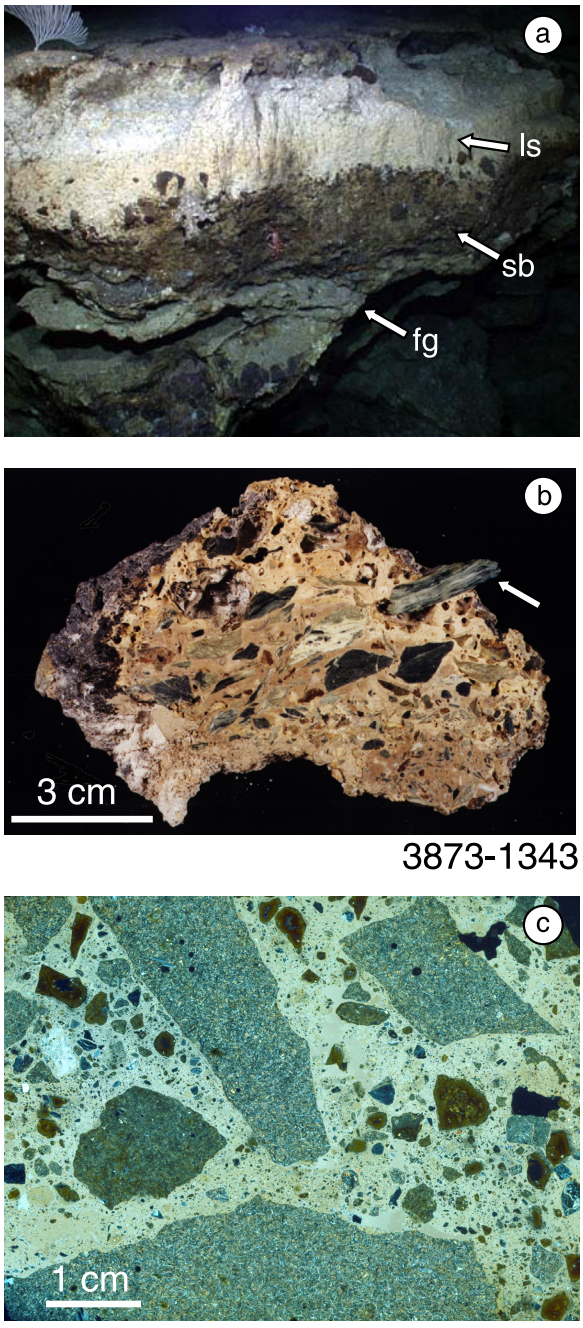

Figure 15. Sedimentary rock units above the DSZ. (a) Strongly foliated serpentinite mylonite and fault gouge (fg) is overlain by dark brown sedimentary breccia (sb) that grades upward into pelagic limestone (ls), *Alvin* 3867 (744 m), 150 m northeast of the LCHF. (b) *Alvin* sample 3873–1343 (922 m) of sedimentary breccia with clasts of mylonitic serpentinite (arrow) and talc-amphibole schist in a light colored, fossil-rich carbonate matrix. (c) Photomicrograph of sedimentary breccia with variably weathered basaltic clasts in a fossil-rich, pelagic carbonate matrix. *Alvin* sample 3865–1250 (796 m). See Table 2 for sample locations.

dispersed on nearby slopes or removed by mass wasting.

[43] The sedimentary section consists of a lower sequence of sedimentary breccias grading upward into pelagic limestone (Table 2). Across most of the south wall exposures, clasts in the breccia become increasingly sparse over an interval <1 m as it grades upward into the pelagic limestone (Figure 15a). The limestone in turn grades upward into unconsolidated pelagic ooze with sparse, scattered, basaltic blocks. Various aspects of samples of these sedimentary rock units have been discussed in previous publications [*Kelley et al.*, 2001b, 2005; *Schroeder et al.*, 2002; *Früh-Green et al.*, 2003]. Here we provide information on the outcrop character, internal structures and contact relationships of these units. The sedimentary section may record an important part of the tectonic history of the massif.

4.5.1. Sedimentary Breccias

[44] The sedimentary breccias are massive to crudely bedded, typically 1–3 m thick, and include both matrix- and clast-supported textures (Table 2). Clasts consist mostly of poorly sorted, angular fragments of massive to mylonitic serpentinite, rare metagabbro, and other hydrothermally altered mineral and lithic clasts. Variably altered basaltic materials dominate some samples. The matrix of the breccia is pink to cream-colored, variably recrystallized, fossil-rich, pelagic carbonate (Figure 15b).

[45] The poorly developed bedding shows only subtle clast-size variations. Meter-scale, fining-upward sequences occur in some places. The bedding generally has a subhorizontal attitude or dips gently to the east or west, roughly conformable with the foliation in the underlying DSZ. Rarely, bedding has been disrupted and tilted to moderate dips near steep faults, for example, near the LCHF. Locally the basal depositional contact of the breccia covers faults and shear zones in the basement (Figure 16) demonstrating that deposition of this unit postdated at least some of the faulting (Figure 17).

4.5.2. Pelagic Limestones

[46] The pelagic limestones lie conformably over the sedimentary breccias (Figure 15a) and are composed of light-colored fossiliferous material that is essentially indistinguishable from the matrix of the breccias. The thickness of this unit ranges from a few tens of centimeters to about 2 meters.

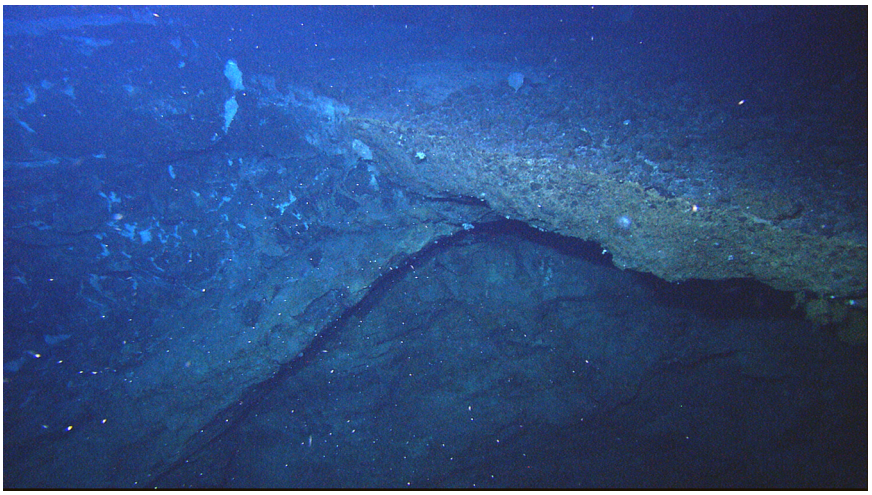

Figure 16. Relationship between shear zones and sedimentary rocks. West-dipping shear zone cuts and deforms the mylonitic rocks of the DSZ, here riddled with white hydrothermal carbonate veins. The shear zone is overlain by a gently east-dipping bed of massive, sedimentary breccia. As inferred from the geological map, deposition of the sedimentary rocks postdates slip on normal slip shear zones and faults in this area. *Hercules* digital image. Horizontal dimension about 4 m. (Image from University of Washington, NOAA, IFE, and University of Rhode Island, IAO).

Thin bedding and laminations are visible in some outcrops. Dark clasts of basement material occur near the gradational basal contact of this unit. Sediment-filled burrows and cracks are also visible. Near the edge of the south wall, widely spaced cracks occur in the upper surface and detached blocks litter the slopes. Near the LCHF, the cracks in the limestone bed are filled with hydrothermal carbonate deposits, some of which protrude upward in delicate finger-like growths.

[47] The composition and age of the sedimentary breccias shed additional light on the evolution of the Atlantis Massif. AMS ^{14}C age-dating of samples of the lithified pelagic carbonate caprocks and carbonate matrix in the sedimentary breccias yielded ages of 25,000 to 34,000 years, which indicates that a number of the carbonate sediments and breccias at the Atlantis Massif were deposited just before the last glacial maximum 20,000 years ago [*Früh-Green et al.*, 2003]. A glacial age of many of the sediment samples is consistent with bulk carbonate $\delta^{18}O$ values higher than ~2‰ (*versus.* vpdb), which may reflect low temperature (~2°–10°C) precipitation from ^{18}O-rich bottom waters during glacial times. The radiocarbon ages of the sedimentary rocks overlap with ages determined on calcite veins in the basement rocks and the oldest vent structures of the LCHF, suggesting that lithification of the sediments was rapid and was enhanced by diffusely percolating, high-pH fluids emanating from the underlying serpentinites [*Schroeder et al.*, 2002; *Früh-Green et al.*, 2003]. Cracks filled with fossiliferous ooze further support the interpretation that deposition, fracturing, and rapid cementation occurred as the sedimentary breccia and overlying limestone were deposited [*Schroeder et al.*, 2002].

5. Evolution of the Atlantis Massif Oceanic Core Complex

[48] In this section we develop a temporal evolution for the south wall of the Atlantis Massif based

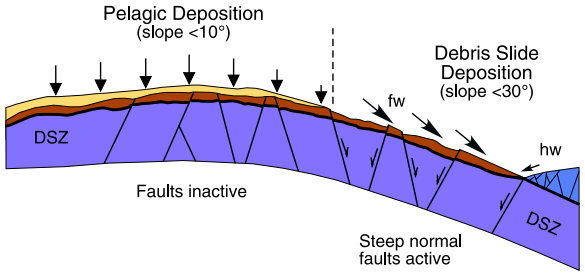

Figure 17. Schematic representation of deposition of sedimentary rock units on top of the DSZ. Sedimentation atop the DSZ (purple) changes from debris slides (orange) to pelagic carbonate (tan) as the shear zone rotates to a horizontal orientation during uplift and movement away from the spreading center. Debris slide material is sourced in both the footwall (serpentinites and metagabbros) and highly fractured hanging wall (basalts, blue).

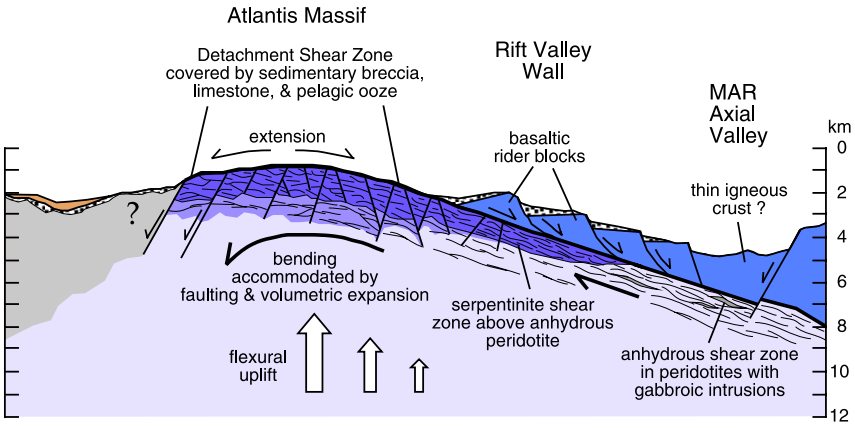

Figure 18. Interpretive cross section of the Atlantis Massif. The oceanic core complex forms as a result of extension, unroofing, and uplift on the edge of the MAR. A major broad shear zone (lined pattern) initially develops beneath the spreading axis where peridotites and gabbroic intrusions are deformed under granulite to amphibolite facies conditions. As the footwall of the shear zone is progressively unroofed and hydrated, a localized DSZ forms in serpentinite mylonites and talc-amphibole-chlorite schists (dark purple). Upper crustal hanging wall rocks (blue) are removed by slip on the moderately dipping DSZ. Bending of the DSZ and reorientation of its internal structures are accommodated by a combination of slip on anastomosing shear zones and steeply dipping normal faults (bold lines) and volumetric expansion related to serpentinization (light purple). Relief created by steep faults is buried by debris slide material and pelagic deposits that accumulate during deformation of the DSZ footwall. Mass wasting along the southern, transform-parallel wall of the massif exploits weak DSZ material as well as late, steep faults where serpentinization and hydrothermal venting are focused. No vertical exaggeration.

on the relative chronology of observed structures (Figure 18). The relative ages of rock units and structures can in most cases be clearly established with crosscutting relationships. The absolute timing of these events is constrained only by the age of the massif inferred from the distance from the spreading axis and the half-spreading rate of 12 mm/yr [*Blackman et al.*, 2002]. A younger limit for the deformation features of the basement of the Atlantis Massif is provided by preliminary radiometric dates of on hydrothermal deposits of the LCHF and carbonate veins and cement sedimentary rocks of a few tens of thousands of years [*Früh-Green et al.*, 2003].

5.1. Mantle Flow and Magmatic Construction

[49] The ultramafic and mafic assemblage found in the basement rocks that dominate the south wall of the massif record the oldest part of the history of the area. In the ultramafic rocks, deformation fabrics typical of those found in residual upper mantle peridotites from the seafloor [*Dick*, 1989] and ophiolites [*Nicolas*, 1989] can still be seen though they are overgrown by lower temperature minerals [*Schroeder and John*, 2004; *Boschi et al.*, 2006]. Gabbroic intrusive bodies were probably intruded beneath the spreading axis (Figure 18). Locally preserved remnants of granulite facies metagabbroic rocks suggest that the intrusions may have occurred during crystal-plastic flow in the surrounding mantle material.

5.2. Deformation, Hydration, and Strain Localization

[50] Although most of the high-temperature history of the ultramafic rocks is obscured by later growth of serpentine minerals, the gabbroic rocks from the south wall record a history of high-temperature hydrous (amphibolite facies) deformation and recrystallization [*Schroeder and John*, 2004; *Boschi et al.*, 2006]. This material is found throughout the south wall exposures indicating that fluids penetrated the deforming ultramafic-mafic assemblage. Under decreasing temperature conditions, relatively weak serpentine, talc, and amphibole assemblages crystallized in shear zones and as strain became localized in the DSZ [*Schroeder and John*, 2004]. Focused slip on the DSZ resulted in the unroofing of the footwall domain of the OCC. The intensely focused deformation and fluid interactions in the DSZ [*Boschi et al.*, 2004; *Schroeder and John*, 2004; *Boschi et al.*, 2006] contrast with the general lack of low-temperature deformation features in the structurally deeper basement rocks. No syntectonic magmatic intrusions have been

found cutting the lower temperature shear zones including the DSZ.

5.3. Coaxial Flattening and Vertical Collapse

[51] By the time the DSZ moved upward and laterally to define the median valley wall of the MAR, the slip on this major shear zone ceased. Continued spreading carried the DSZ westward where it was rotated progressively to subhorizontal and eventually a west-dipping orientation.

[52] The only remnants of the hanging wall domain are fractured basaltic lavas found on the eastern edges of the massif several kilometers away from the south wall study area [*Cann et al.*, 1997; *Blackman et al.*, 2002]. Mantle peridotites and high-temperature metagabbros have been juxtaposed with these basaltic lavas. The thickness and composition of any other crustal material that was removed by faulting is not known. In addition, about 4000 m of uplift would have to occur if the seafloor moved along a flow line from the deep median valley of the MAR near the RTI to the present depth of the Atlantis Massif over less than 10 km laterally. Taken together, these relationships make it very likely that the DSZ once dipped relatively steeply beneath the median valley. Slip on only a low-angle surface would be unlikely to bring deep level rocks to the surface and to the elevation of the top of the massif in this short distance. Thus the shear zone probably rotated into its present low-angle, arched form by later deformation. Insufficient data are available at present to place additional constraints on this process.

[53] The internal structure of the DSZ confirms the expected normal (top-toward-the-axis) sense of shear for an oceanic detachment shear zone. The shear zone is laterally extensive but limited to only a thickness of 100 m of the upper surface, implying strong localization of strain. Although there is no strongly corrugated surface immediately adjacent to the shear zone, it is reasonable to project this structure northward or eastward beneath the corrugated and striated top of the massif (Figure 2) [*Blackman et al.*, 2002].

[54] The localized shear zones in the footwall of the OCC postdate and overlap in time with the fabrics in the DSZ. Thus there appears to be a transition from focused slip on the DSZ to more widely distributed deformation on the discrete shear zones. The shear zones dip both toward and away from the axis (and in some cases toward the Atlantis Transform Fault), indicating a component of coaxial strain or vertical flattening of the footwall beneath the DSZ. Significant volume changes associated with serpentinization probably also contributed to uplift and accommodation of footwall deformation that ultimately brought the DSZ into a subhorizontal orientation.

5.4. Late Faulting

[55] The steep normal faults that create marked lineaments in the bathymetry (e.g., Figure 4) are relatively young features, but the geological relationships with the sedimentary units suggest that they are not simply active faults related to the present tectonic regime. The sedimentary units above the DSZ appear to bury relief created by the steep faults mapped on the south wall. Because the breccias were deposited when the DSZ had a more steeply dipping orientation, probably when it defined the median valley wall, these faults (that disrupt the breccias in only one place) must have formed before the DSZ rotated to a lower angle orientation. Therefore they may also have been rotated similarly. Reactivation and exploitation of these faults by mass wasting are very recent events that appear to be closely related to the localization and maintenance of flow at the LCHF.

5.5. Stratigraphic Record of Footwall Deformation

[56] The composition and stratigraphic relations of the sedimentary section on the top of the south wall of the Atlantis Massif may hold important clues to the tectonic evolution of the DSZ and the core complex in general. The composition and texture of the sedimentary units suggests a change from deposition of coarse, proximal clastic material in a steep, tectonically active terrain to accumulations of increasingly pelagic deposits across a low-relief surface. The sedimentary breccias were derived from both footwall (ultramafic and mafic basement) and hanging wall (basaltic) source areas and deposited as debris slides and talus accumulations, and yet, no hanging wall material crops out nearby and there is presently no substantial relief of the ultramafic and mafic basement terrane that could have served as a source area. We interpret the change from coarse clastic to pelagic deposition to reflect changes in the overall depositional regime of the footwall of the core complex as the DSZ rotated from a relatively steeply dipping median valley wall to the subhorizontal upper

surface of the massif as it moved laterally away from the spreading axis (Figure 17).

[57] The basal contact of the sedimentary unit indicates that the DSZ was exposed on the seafloor where the overlying coarse-grained materials were deposited. Fractures in the DSZ in-filled by material similar to the matrix of the breccias [*Schroeder et al.*, 2002; *Früh-Green et al.*, 2003] probably formed at this time. Low-angle unconformities along this contact may reflect mass wasting or erosion of the DSZ surface, or local, predepositional truncations of the shear zone fabric by low-angle faulting. Significantly, both units of the sedimentary section were deposited on surfaces that are subparallel to the shear zone fabric of the DSZ. Thus the depositional regime reflects the slope and relief of the DSZ surface.

[58] The coarse, polymictic, sedimentary breccias indicate a period of deposition when the DSZ had substantially more relief and a steeper slope than present. Debris slide and talus deposits similar to the sedimentary breccias dominate moderately sloping terrain of rift valleys and transform faults of the Mid-Atlantic Ridge [*Karson and Dick*, 1983; *Tucholke et al.*, 1997; *Gao et al.*, 1998]. On slopes greater than about 30°, active mass wasting dominates. On slopes less than about 30° substantial volumes of rock debris begin to accumulate [e.g., *Karson and Dick*, 1983]. Following this general observation, we infer that the dip of the DSZ was about 30° or less as the sedimentary breccia unit began to accumulate on top of it.

[59] The pelagic limestone must have accumulated atop the sedimentary breccia after the depositional slope and relief had decreased substantially, probably to less than 10°. This surface remained essentially parallel to the DSZ. Thus the clastic to pelagic transition in this sequence may be the stratigraphic expression of the flattening of the detachment shear zone as the massif moved laterally away from the spreading axis. Similar rotation to a subhorizontal orientation of originally more steeply dipping detachment shear zones is commonly inferred for continental core complexes [*Spencer*, 1984; *Davis et al.*, 1986; *Wernicke and Axen*, 1988]. This interpretation is consistent with active depositional regimes on the present median valley walls of the MAR, some of which feature active mass wasting and debris slide deposition on similar detachment shear zones [*Karson and Lawrence*, 1997a, 1997b]. It also explains the lack of relief and source materials for the sedimentary breccias at the present stage of evolution of the massif.

6. Discussion

[60] Geological relationships exposed on the south wall of the Atlantis Massif provide new insights into the evolution of this OCC that may apply to other similar massifs. These results have been possible only because of the extensive investigations at various scales that we were able to carry out and because of the excellent exposures available on the south wall of the massif. This exposure of the OCC footwall domain may be especially good because of active mass wasting that has created many steep cliffs that expose cross sections of the basement, DSZ and sedimentary cover of the massif.

6.1. Variations Across the Atlantis Massif

[61] Results from our investigations on the south wall of the Atlantis Massif suggest a very different geologic structure and tectonic evolution than that inferred for the central part of the massif. These differences must be reconciled in order to understand the evolution of the massif as a whole.

[62] Despite obvious differences between submersible investigations of extensive escarpments south wall and nearly continuous, but essentially one-dimensional drilling in the central part of the massif, it is clear that there are significant differences between these two areas (Figures 2 and 18). The proportion of ultramafic material on the south wall (~70%) is much greater than that found during drilling in the central part of the Atlantis Massif (<5%) [*Shipboard Scientific Party*, 2005a, 2005b]. Furthermore, the protoliths of the south wall ultramafic rocks are residual upper mantle peridotites, whereas most of the ultramafic material from Hole U1309D is "dunitic troctolite," probably of magmatic origin [*Shipboard Scientific Party*, 2005b]. It is not clear if this variation is part of a regional trend related to decreased magma production toward the Atlantis Transform Fault [*Stroup and Fox*, 1981; *Karson et al.*, 1987; *Cannat*, 1993] or merely a reflection of local variations in a highly heterogeneous mafic-ultramafic assemblage.

[63] OCCs have apparently formed in a number of different tectonic settings with respect to spreading center segmentation and magma supply [*Karson*, 1998, 1999; *Dick et al.*, 2000; *MacLeod et al.*, 2002]. So it may not be surprising that significant variations of this type occur even within a single

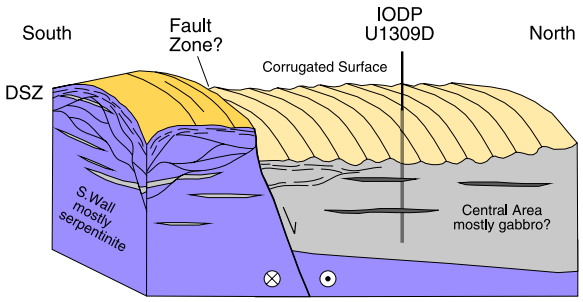

Figure 19. Schematic diagram showing possible relationship between features found on the south wall and those found in the central part of the Atlantis Massif. IODP Hole U1309D (1656 mbsl) penetrated >1400 m of variably deformed and altered gabbroic (gray) and minor ultramafic (dark gray) igneous rocks beneath the corrugated surface (detachment fault?). The south wall is dominantly serpentinized residual mantle peridotite (purple) with lesser metagabbroic rocks (light gray) capped by a ~100-m-thick detachment shear zone (DSZ). The contact between these two terranes may be a fault (as shown), an igneous contact (southern limit of gabbroic material), or a combination of these. See text for discussion.

OCC massif. OCCs that resemble the south wall of the Atlantis Massif, with dominantly residual upper mantle material, for example, OCC at 15°45′N on the MAR), might be interpreted as having formed under essentially amagmatic conditions [*MacLeod et al.*, 2002; *Shipboard Scientific Party*, 2004]. The central part of the Atlantis Massif is more like other OCCs composed of gabbroic material with synkinematic intrusions, for example, OCCs on the Southwest Indian Ridge [*Dick et al.*, 2000] or the MARK Area [*Cannat et al.*, 1995a]. Following these interpretations, different parts of the Atlantis Massif would have developed in very different thermal, magmatic, and mechanical regimes, and yet side-by-side.

[64] The significant differences between the south wall and the central parts of the massif suggest that there must be a major discontinuity between these areas. The boundary between these areas might be essentially an igneous contact defined by the southern limit of gabbro intrusion(s). Alternatively, it might be a fault zone (Figure 19). A major east-west scarp bounding the northern edge of the southern ridge may mark the location of this boundary. Considering the dominant rock types to the north and south, it is likely that this would have a component of down-to-north movement. It is also possible that it could be a lateral ramp linking separate detachment systems.

6.2. Detachment Faults and Corrugated Surfaces

[65] Despite being located on an extensive corrugated surface interpreted as a major detachment fault, IODP Hole 1309D did not document a major low-angle shear zone, though numerous small-scale shear zones were recovered and local occurrences of talc-rich rocks were observed [*Shipboard Scientific Party*, 2005a]. Even considering the relatively low recovery of material near the top of the hole, it is not likely that a 100 m thick DSZ, as found on the south wall is present. The DSZ on the south wall is part of a distinctive structural assemblage and similar assemblages may have been sampled in other OCCs of the MAR [*MacLeod et al.*, 2002; *Escartín et al.*, 2003; *Shipboard Scientific Party*, 2004].

[66] Although detachment faults or shear zones have been inferred from the exposure of plutonic rocks, from the morphology of corrugated surfaces [*Cann et al.*, 1997; *Tucholke et al.*, 1998; *Reston et al.*, 2002] and from drilling results [*MacLeod et al.*, 2002], this is the first time a major subhorizontal detachment shear zone has been mapped continuously for kilometers along the top edge of an OCC. Projecting this shear zone northward to the corrugated and striated surface of the central part of the massif helps corroborate the widespread belief that this distinctive morphology can be interpreted as major detachment faults or shear zones. The exact nature of the corrugations is not yet documented.

[67] Faults and discrete centimeter- to meter-scale serpentinite shear zones have been found in ultramafic rocks of other OCC collected by drilling [*Cannat et al.*, 1995b; *Shipboard Scientific Party*, 2004] and near-bottom studies [*Mével et al.*, 1991; *Cannat et al.*, 1997; *Karson and Lawrence*, 1997a; *Lagabrielle et al.*, 1998; *Karson*, 1999; *MacLeod et al.*, 2002]. Our results show that these types of ductile shear zones can be very widespread through the footwall of an OCC and that isolated samples of sheared serpentinite do not in themselves necessarily indicate the proximity of a major detachment shear zone. Geologic mapping will be required to document continuous detachment shear zones in other OCCs.

7. Conclusions

[68] Building on the results of previous studies we have used new near-bottom data to shed light on the internal structure of a cross section of the

Atlantis Massif oceanic core complex. We have exploited a major tectonic escarpment facing the Atlantis Transform Fault to investigate the details of the footwall domain of this highly extended oceanic terrane. From our investigation we draw the following conclusions:

[69] 1. Geologic mapping shows that most of the south wall of the Atlantis Massif is composed of variably serpentinized residual upper mantle peridotites and lesser gabbroic intrusions. This contrasts sharply with the results of IODP drilling <10 km to the north where a thick sequence of mainly gabbroic rocks was recovered. This lithologic difference suggests that there is a major geologic boundary between these two areas, probably at the north edge of the southern ridge, which is marked by a pronounced change in bathymetry.

[70] 2. Massive ultramafic and mafic rocks have a thickness of >3000 m on the south wall of the massif. Narrow shear zones cut this assemblage.

[71] 3. The top of the south wall features a ~100-m-thick detachment shear zone (DSZ) composed of intensely deformed and metasomatized ultramafic and lesser mafic rocks with a very strong, outcrop-scale foliation. The shear zone has been traced for more than 3 km along the crest of the massif.

[72] 4. Mylonites and schists of the DSZ have kinematic indicators showing consistent top-to-east (toward the spreading center) sense of displacement. Large noncoaxial strains inferred for the DSZ are consistent with its origin as the manifestation of localized tectonic extension during the evolution of the massif.

[73] 5. A crosscutting array of anastomosing shear zones consistently show normal slip and collectively appear to accomplish a coaxial deformation resulting in vertical flattening of the footwall domain. This deformation could have resulted in the rotation of the DSZ from at least a moderate dip toward the ridge axis into its present, gently dipping, arched form.

[74] 6. Late normal faults provide permeable pathways for hydrothermal circulation, most evident near the Lost City Hydrothermal Field (LCHF). They frame a kilometer-scale, down-dropped block that hosts the LCHF and also localize mass wasting across the top of the south wall.

[75] 7. A thin (few meters) sequence of distinctive sedimentary rocks directly overlies the DSZ at the top of the south wall and may extend over much of the massif. This sequence of sedimentary breccias grading upward into pelagic limestone postdate all basement deformation structures except a few of the latest normal faults. The composition and textures of these rocks shows a change from debris slide to pelagic sedimentation that may reflect the rotation of the DSZ from a moderately to gently dipping orientation during deformation of the footwall of the DSZ.

[76] The integrated results of the investigations of the Atlantis Massif to date emphasize the need for comprehensive studies of OCCs. The current understanding of the evolution of this massif has required constraints from many different disciplines and across a range of scales. Investigations of other OCCs, and even other parts of the Atlantis Massif, have shown that major differences in composition and structure exist on scales of tens of meters to kilometers among and within these complex terranes. They continue to challenge our understanding of the interplay of magmatism, metamorphism, and tectonics at mid-ocean ridge spreading centers.

Acknowledgments

[77] We thank the captains, crews, and technical staffs for *Alvin*, *Argo II*, and *ABE* aboard R/V *Atlantis* during cruises AT3-60 and AT7-34 to the Atlantis Massif in 2000 and 2003 for their outstanding support of this project. We also thank Chiara Boschi, Adélie Delacour, and Kris Ludwig for sharing their data on the rocks and the scientific parties from these cruises for their many contributions to the data collection and discussions at sea. *Hercules* images were provided courtesy of NOAA Lost City Exploration Program, University of WA, NOAA, Institute for Exploration, and University of RI, Institute for Archaeological Oceanography. Reviews by Brian Tucholke and an anonymous reviewer helped focus and improve the presentation. This work was supported by NSF grants OCE-9712430 and 0136816 to Karson and Kelley and Swiss SNF grant 2100-068055 to Früh-Green.

References

Berthe, D., P. Choukroune, and P. Jegouzo (1979), Orthogneiss, mylonite and noncoaxial deformation of granites: The example of the South American shear zone, *J. Struct. Geol.*, *1*, 31–42.

Blackman, D. K., J. R. Cann, B. Janssen, and D. K. Smith (1998), Origin of extensional core complexes: Evidence from the Mid-Atlantic Ridge at Atlantis fracture zone, *J. Geophys. Res.*, *103*, 21,315–21,334.

Blackman, D. K., D. S. Kelley, J. A. Karson, and Shipboard Scientific Party (2001), Seafloor mapping and sampling of the MAR 30°N oceanic core complex—MARVEL (Mid-Atlantic Ridge Vents in Extending Lithosphere) 2000, *InterRidge Newsl.*, *10*, 33–36.

Blackman, D. K., et al. (2002), Geology of the Atlantis Massif (Mid-Atlantic Ridge, 30°N): Implications for the evolution of an ultramafic oceanic core complex, *Mar. Geophys. Res.*, *23*, 443–469.

Boschi, C., G. L. Früh-Green, and D. S. Kelley (2003), Links between tectonic and serpentinization processes and their consequences for hydrothermal activity (Atlantis Massif, MAR 30°N), *Geophys. Res. Abstr.*, *5*, 09796.

Boschi, C., G. L. Früh-Green, J. A. Karson, D. S. Kelley, A. Dini, and A. G. Delacour (2004), Mass transfer and metasomatism during the tectonic evolution of the Atlantis Massif (30°N MAR), paper presented at 32nd International Geological Congress, Int. Union of Geol. Sci., Florence, Italy.

Boschi, C., G. L. Früh-Green, A. Delacour, J. A. Karson, and D.S. Kelley (2006), Mass transfer and fluid flow during detachment faulting and development of an oceanic core complex, Atlantis Massif (MAR 30°N), *Geochem. Geophys. Geosyst.*, *7*, Q01004, doi:10.1029/2005GC001074.

Canales, J. P., B. E. Tucholke, and J. A. Collins (2004), Seismic reflection imaging of an oceanic detachment fault: Atlantis megamullion (Mid-Atlantic Ridge, 30°10′N), *Earth Planet. Sci. Lett.*, *222*, 543–560.

Cann, J. R., D. K. Blackman, D. K. Smith, E. McAllister, B. Janssen, S. Mello, E. Avgerinos, A. R. Pascoe, and J. Escartín (1997), Corrugated slip surfaces formed at ridge-transform intersections on the Mid-Atlantic Ridge, *Nature*, *385*, 329–332.

Cannat, M. (1993), Emplacement of mantle rocks in the sea floor at mid-ocean ridges, *J. Geophys. Res.*, *98*, 4163–4172.

Cannat, M., J. A. Karson, D. J. Miller, and ODP Leg 153 Shipboard Scientific Party (1995a), Probing the plutonic foundation of the Mid-Atlantic Ridge, *Eos Trans. AGU*, *76*, 129–133.

Cannat, M., et al. (1995b), *Proceedings of the Ocean Drilling Program, Initial Reports*, vol. 153, 798 pp., Ocean Drill. Program, College Station, Tex.

Cannat, M., Y. Lagabrielle, N. de Coutures, H. Bougault, J. Casey, L. Dmitriev, and Y. Fouquet (1997), Ultramafic and gabbroic exposures at the Mid-Atlantic Ridge: Geological mapping in the 15°N region, *Tectonophysics*, *279*, 193–214.

Collins, J. A., B. E. Tucholke, and J. P. Canales (2001), Structure of Mid-Atlantic Ridge megamullions from seismic refraction experiments and multichannel seismic reflection profiling, *Eos Trans. AGU*, *82*(47), Fall. Meet. Suppl., Abstract T11C-0865.

Curless, B., and M. Levoy (1996), A volumetric method for building complex models from range images, *Comput. Graphics*, *30*, 303–312.

Davis, G. A., G. S. Lister, and S. R. Reynolds (1986), Structural evolution of the Whipple and South Mountain shear zones, southwestern United States, *Geology*, *14*, 7–10.

Dick, H. J. B. (1989), Abyssal peridotites, very slow spreading ridges and ocean ridge magmatism, in *Magmatism in the Ocean Basins*, edited by A. D. Saunders and M. J. Norry, *Geol. Soc. Spec. Publ.*, *42*, 71–105.

Dick, H. J. B., P. Meyer, S. Bloomer, S. Kirby, D. Stakes, and C. Mawer (1991), Lithostratigraphic evolution of an in situ section of oceanic layer 3, *Proc. Ocean Drill. Program Sci. Results*, *118*, 439–515.

Dick, H. J. B., et al. (2000), A long in situ section of the lower oceanic crust: Results of ODP Leg 176 drilling at the Southwest Indian Ridge, *Earth Planet. Sci. Lett.*, *179*, 31–51.

Escartín, J., and M. Cannat (1999), Ultramafic exposures and the gravity signature of the lithosphere near the Fifteen-Twenty Fracture Zone (Mid-Atlantic Ridge, 14°–16.5°N), *Earth Planet. Sci. Lett.*, *171*, 411–424.

Escartín, J., C. Mével, C. J. MacLeod, and A. M. McCaig (2003), Constraints on deformation conditions and the origin of oceanic detachments: The Mid-Atlantic Ridge core complex at 15°45′N, *Geochem. Geophys. Geosyst.*, *4*(8), 1067, doi:10.1029/2002GC000472.

Früh-Green, G. L., D. S. Kelley, J. A. Karson, D. K. Blackman, C. Boschi, B. E. John, T. Schroeder, and D. K. Ross (2001), Hydrothermal alteration, serpentinization and carbonate precipitation at the Lost City Vent Field (30°N, Mid-Atlantic Ridge), *Eos Trans. AGU*, *82*(47), Fall. Meet. Suppl., Abstract T11C-0869.

Früh-Green, G. L., C. Boschi, D. S. Kelley, J. A. D. Connolly, and M. O. Schrenk (2002), The role of serpentinization in metasomatism, carbonate precipitation and microbial activity: Stable isotope constraints from the Lost City Vent Field (MAR 30°N), *Eos Trans. AGU*, *83*(47), Fall Meet. Suppl., Abstract V72A-1289.

Früh-Green, G. L., D. S. Kelley, S. M. Bernasconi, J. A. Karson, K. A. Ludwig, D. A. Butterfield, C. Boschi, and G. Proskuroski (2003), 30,000 years of hydrothermal activity at the Lost City vent field, *Science*, *301*, 495–498.

Gao, D., S. D. Hurst, J. A. Karson, J. R. Delaney, and F. N. Spiess (1998), Computer-aided interpretation of side-looking sonar images from the eastern intersection of the Mid-Atlantic Ridge with the Kane transform, *J. Geophys. Res.*, *103*, 20,997–21,014.

Hurst, S. D., J. A. Karson, and K. L. Verosub (1994), Paleomagnetic study of tilted diabase dikes in fast-spread oceanic crust exposed at Hess Deep, *Tectonics*, *13*, 789–802.

Karson, J. A. (1990), Seafloor spreading on the Mid-Atlantic Ridge: Implications for the structure of ophiolites and oceanic lithosphere produced in slow-spreading environments, in *Ophiolites and Oceanic Crustal Analogues: Proceedings of the Symposium "Troodos 1987"*, edited by J. Malpas et al., pp. 125–130, Geol. Surv. Dep., Nicosia, Cyprus.

Karson, J. A. (1998), Internal structure of oceanic lithosphere: A perspective from tectonic windows, in *Faulting and Magmatism at Mid-Ocean Ridges*, *Geophys. Monogr. Ser.*, vol. 106, edited by W. R. Buck et al., pp. 177–218, AGU, Washington, D. C.

Karson, J. A. (1999), Geological investigation of a lineated massif at the Kane transform: Implications for oceanic core complexes, *Philos. Trans. R. Soc. London, Ser. A*, *357*, 713–740.

Karson, J. A., and H. J. B. Dick (1983), Tectonics of ridge-transform intersections at the Kane Fracture Zone, 24°N on the Mid-Atlantic Ridge, *Mar. Geophys. Res.*, *6*, 51–98.

Karson, J. A., and R. M. Lawrence (1997a), Tectonic setting of serpentinite exposures on the western median valley wall of the MARK Area in the vicinity of Site 920, *Proc. Ocean Drill. Program Sci. Results*, *153*, 5–22.

Karson, J. A., and R. M. Lawrence (1997b), Tectonic window into gabbroic rocks of the middle oceanic crust in the MARK area near Sites 921–924, *Proc. Ocean Drill. Program Sci. Results*, *153*, 61–76.

Karson, J. A., et al. (1987), Along-axis variations in seafloor spreading in the MARK area, *Nature*, *328*, 681–685.

Kelley, D., et al. (2001a), Discovery of Lost City: An off-axis, peridotite-hosted, hydrothermal field near 30°N on the Mid-Atlantic Ridge, *RIDGE Events Newsl.*, *11*, 3–9.

Kelley, D. S., et al. (2001b), An off-axis hydrothermal vent field near the Mid-Atlantic Ridge at 30°N, *Nature*, *412*, 145–149.

Kelley, D. S., et al. (2005), A serpentinite-hosted ecosystem: The Lost City Hydrothermal Field, *Science*, *307*, 1428–1434.

Lagabrielle, Y., D. Bideau, M. Cannat, J. A. Karson, and C. Mével (1998), Ultramafic-mafic plutonic rock suites exposed along the Mid-Atlantic Ridge (10°N–30°N): Symmetrical-asymmetrical distribution and implications for seafloor spreading processes, in *Faulting and Magmatism at Mid-Ocean Ridges*, *Geophys. Monogr. Ser.*, vol. 106, edited by W. R. Buck et al., pp. 153–176, AGU, Washington, D. C.

Lister, G. S., and A. W. Snoke (1984), S-C mylonites, *J. Struct. Geol.*, *6*, 617–638.

MacLeod, C. J., et al. (2002), Direct geological evidence for oceanic detachment faulting: The Mid-Atlantic Ridge, 15°45′N, *Geology*, *30*, 879–882.

Mével, C., M. Cannat, P. Gente, E. Marion, J.-M. Auzende, and J. A. Karson (1991), Emplacement of deep crustal and mantle rocks on the West Median Valley Wall of the MARK Area (M. A. R. 23°N), *Tectonophysics*, *190*, 31–53.

Mutter, J. C., and J. A. Karson (1992), Structural processes at slow-spreading ridges, *Science*, *257*, 627–634.

Nicolas, A. (1989), *Structure of Ophiolites and Dynamics of Oceanic Lithosphere*, 367 pp., Springer, New York.

Okino, K., K. Matsuda, D. M. Christie, Y. Nogi, and K. Koizumi (2004), Development of oceanic detachment and asymmetric spreading at the Australian-Antarctic Discordance, *Geochem. Geophys. Geosyst.*, *5*, Q12012, doi:10.1029/2004GC000793.

Passchier, C. W., and C. Simpson (1986), Porphyroclast systems as kinematic indicators, *J. Struct. Geol.*, *8*, 831–843.

Ramsay, J. G., and R. H. Graham (1970), Strain variations in shear belts, *Can. J. Earth Sci.*, *7*, 786–813.

Reston, T. J., W. Weinrebe, I. Grevemeyer, E. R. Flueh, N. C. Mitchell, L. Kirstein, C. Kopp, and Participants of Meteor 47/2 (2002), A rifted inside corner massif on the Mid-Atlantic Ridge at 5°S, *Earth Planet. Sci. Lett.*, *200*, 255–269.

Schroeder, T., and B. E. John (2004), Strain localization on an oceanic detachment fault system, Atlantis Massif, 30°N, Mid-Atlantic Ridge, *Geochem. Geophys. Geosyst.*, *5*, Q11007, doi:10.1029/2004GC000728.

Schroeder, T., B. E. John, and B. R. Frost (2002), Geologic implications of seawater circulation through peridotite exposed at slow-spreading mid-ocean ridges, *Geology*, *30*, 367–370.

Searle, R. C., M. Cannat, K. Fujioka, C. Mével, H. Fujimoto, A. Bralee, and L. Parson (2003), FUJI Dome: A large detachment fault near 64°E on the very slow-spreading southwest Indian Ridge, *Geochem. Geophys. Geosyst.*, *4*(8), 9105, doi:10.1029/2003GC000519.

Shipboard Scientific Party (2004), *Proceedings of Ocean Drilling Program, Initial Reports*, vol. 209, Ocean Drill. Program, College Station, Tex. (Available at http://www-odp.tamu.edu/publications/209_IR/209ir.htm)

Shipboard Scientific Party (2005a), Expedition 304 Preliminary Report: Oceanic Core Complex Formation, Atlantis Massif, Integrated Ocean Drill. Program, College Station, Tex. (Available at http://iodp.tamu.edu/publications/PR/304PR/304PR.html)

Shipboard Scientific Party (2005b), Expedition 305 Preliminary Report: Oceanic Core Complex Formation, Atlantis Massif, Integrated Ocean Drill. Program, College Station, Tex. (Available at http://iodp.tamu.edu/publications/PR/305PR/305PR.html)

Simpson, C., and S. M. Schmid (1983), An evaluation of criteria to deduce the sense of movement in sheared rocks, *Geol. Soc. Am. Bull.*, *94*, 1281–1288.

Spencer, J. (1984), The role of tectonic denudation in warping and uplift of low-angle normal faults, *Geology*, *12*, 95–98.

Stroup, J. B., and P. J. Fox (1981), Geologic investigations in the Cayman Trough: Evidence for thin crust along the Mid-Cayman Rise, *J. Geol.*, *89*, 395–420.

Treves, B., and G. D. Harper (1994), Exposure of serpentinites on the ocean floor: Sequence of faulting and hydrofracturing in the northern Apennine ophicalcites, *Ofioliti*, *19b*, 435–466.

Tucholke, B. E., W. K. Stewart, and M. C. Kleinrock (1997), Long-term denudation of ocean crust in the central North Atlantic Ocean, *Geology*, *25*, 171–174.

Tucholke, B. E., J. Lin, and M. C. Kleinrock (1998), Megamullions and mullion structure defining oceanic metamorphic core complexes on the Mid-Atlantic Ridge, *J. Geophys. Res.*, *103*, 9857–9866.

Tucholke, B. E., K. Fujioka, T. Ishihara, G. Hirth, and M. Kinoshita (2001), Submersible study of an oceanic megamullion in the central North Atlantic, *J. Geophys. Res.*, *106*, 16,145–16,161.

Wernicke, B., and G. J. Axen (1988), On the role of isostacy in the evolution of normal fault systems*Geology*, *16*, 848–851.

White, G. W., and J. B. Stroup (1979), Distribution of rock types in the Mid-Cayman Rise, Caribbean Sea as evidence for conjugate normal faulting in slowly spreading ridges, *Geology*, *7*, 32–36.